IEEE Access
Multidisciplinary ⋮ Rapid Review ⋮ Open Access Journal

Received October 27, 2020, accepted November 14, 2020, date of publication November 24, 2020,
date of current version December 9, 2020.

Digital Object Identifier 10.1109/ACCESS.2020.3039799

Adjacent Channel Compatibility Evaluation and Interference Mitigation Technique Between Earth Station in Motion and IMT-2020

HYUN-KI KIM, (Student Member, IEEE), YEONGI CHO, (Student Member, IEEE), AND HAN-SHIN JO, (Member, IEEE)

Department of Electronics and Control Engineering, Hanbat National University, Daejeon 34158, South Korea

Corresponding author: Han-Shin Jo (hsjo@hanbat.ac.kr)

This work was supported in part by the National Research Foundation of Korea funded by the Korea Government, Ministry of Science and ICT (MSIT), under Grant 2019R1A2C4070361, and in part by the Institute for Information and Communications Technology Promotion Grant funded by the Korea government (MSIT) (Cross layer design of cryptography and physical layer security for IoT networks) under Grant B0722-16-0006.

ABSTRACT The millimeter wave band is becoming popular for mobile broadband usage such as fifth-generation (5G) mobile and mobile satellite services utilizing earth stations in motion (ESIM). According to the 2019 World Radiocommunication Conference (WRC-19), the 5G and ESIM systems will operate in adjacent frequency bands bounded by 27.5 GHz; therefore, the adjacent channel compatibility between ESIM and 5G should be verified. Both, the minimum coupling loss (MCL) and Monte-Carlo (MC) methods are applied to assess the worst and most practical interference effects, respectively, for all types of ESIM including the following: maritime ESIM (M-ESIM), land ESIM (L-ESIM), and aeronautical ESIM (A-ESIM). The distance and guard band between the two systems are indicated by the compatibility conditions. In addition to the conventional interference-to-noise ratio (I/N), the throughput loss of a 5G system is proposed to assess the performance degradation caused by the ESIM interference. Two orthogonal frequency division multiplexing (OFDM) waveforms are proposed to suppress ESIM power leakage into an adjacent channel. A mathematical expression regarding the power spectral density (PSD) and frequency dependent rejection (FDR) is derived for these waveforms, suggesting that the interference can be alleviated. A measured single carrier waveform of a commercial ESIM equipment is used as the benchmark against the proposed OFDM waveforms. The windowed OFDM is able to reduce the guard band by 50–77%. The results obtained for various elevation angles of the ESIM antenna are determined to be applicable to various regions globally.

INDEX TERMS Adjacent channel compatibility, spectral coexistence study, fifth-generation (5G) cellular mobile communications, earth station in motion (ESIM), fixed satellite service (FSS), orthogonal frequency division multiplexing (OFDM), CP-OFDM, windowed OFDM, power spectral density, frequency dependent rejection, minimum coupling loss (MCL), Monte-Carlo (MC).

I. INTRODUCTION

A. BACKGROUND OF COEXISTENCE STUDY

The earth station in motion (ESIM) service is one of the advanced satellite communications systems that is mounted on ships, aircraft, and land vehicles to provide wireless communication and networks. Existing similar systems have offered wireless services to mobile platforms such as aircraft and ships where the use of a fixed satellite service (FSS) network in the range of 3400–4800 MHz (C-band) and 10.7–14.5 GHz (Ku-band) is restricted [1]. However, these systems have the disadvantage of providing a significantly slower transmission rate as the number of users increase. The ESIM consists of relatively small-sized terminals with high precision tracking capabilities associated with state-of-the-art Ka-band satellites providing high-power multiple spot beam coverage in the FSS network, which is expected to have transmission rates of 10–50 Mbits/s [2].

The associate editor coordinating the review of this manuscript and approving it for publication was Danping He.

This work is licensed under a Creative Commons Attribution 4.0 License. For more information, see https://creativecommons.org/licenses/by/4.0/

Recognizing the need for ESIM, the 2015 World Radiocommunication Conference (WRC-15) adopted radio regulations (RR), No.5.527A and Resolution 156, specifying conditions for the use of the 19.7–20.2 GHz and 29.5–30.0 GHz bands by ESIM with certain geostationary orbit satellite (GSO) FSS space stations [3]. In addition, as the demand for broadband connectivity increased, WRC-15 adopted the WRC-19 agenda item 1.5 to consider the operation of the ESIM in the 17.7–19.7 GHz (space to earth) and 27.5–29.5 GHz (earth to space) range [4]. The ESIM is classified into maritime ESIM (M-ESIM), land ESIM (L-ESIM), and aeronautical ESIM (A-ESIM) depending on the environment in which it is operated. In the International Telecommunication Union Radiocommunication (ITU-R) working party (WP) 4A, frequency sharing analysis has been performed for each type of ESIM in the above bands [5]. According to the final acts of the WRC-19, the frequency bands of 27.5–29.5 GHz and 17.7–19.7 GHz are allocated to terrestrial and space services used by various systems; these existing services and their future development needs to be protected from the ESIM system by adopting Resolution 169 [6]. However, it does not contain information regarding adjacent bands.

International Mobile Telecommunication 2020 (IMT-2020) is the official name of fifth-generation (5G) mobile communication as defined by the ITU. The IMT-2020 is expected to be commercialized in 2020 with performance including high data rates, ultra-reliable and low latency communications (URLLC), enhanced mobile broadband (eMBB), and massive machine-type communications (mMTC) [7]. The ITU proposed 11 new possible bands, which ranges from 24.25–86 GHz for IMT-2020 on a primary basis. At the WRC-15, WRC-19 agenda item 1.13 was adopted to determine a suitable frequency band for these potential bands in the IMT-2020 [8]. Therefore, the ITU established a task group, 5/1 (TG 5/1), to confirm the frequency sharing possibility through an interference analysis study between IMT-2020 and the incumbent systems. Considering the 24.25–27.5 GHz band as a possibility, the TG 5/1 performed the interference analysis between IMT-2020 and FSS. Most of the studies indicated that both systems can share frequency on the co-channel [9]. Eventually, 24.25-27.5 GHz was designated as a global 5G frequency in WRC-19.

In order to commercialize the wireless communication systems, interference analysis with the incumbent system must be performed. The interference analysis is generally based on the following two methods: minimum coupling loss (MCL), which is the simplest method with strict assumptions of radio interference power for strictly protecting victim system, and Monte-Carlo (MC), which is a stochastic method with practical assumptions for reasonable spectral coexistence.

The MCL sets the coupling loss between the interferer system and the victim system to the minimum [10]. This is equivalent to assuming the maximum interference power, which is unlikely to occur in a real environment. Nevertheless, the MCL method can provide an approximate prediction of the radio interference power in a short period of time. The results of the MCL analysis determine values such as the minimum separation distance and frequency gap. This mainly deals with one-to-one scenarios, which are interference situations where a single interferer system and victim system are distributed.

In the interference analysis, the MC method is mainly applied in an environment where multiple interferer systems or victim systems are distributed. This method predicts the interference power by applying probabilistic and statistical factors in a practical environment, which is more difficult to analyze than the MCL and requires an accurate scenario assumption [10]. The results are different for each simulation due to the probabilistic factors. Therefore, a sufficient number of simulations are required to obtain reliable data, and the interference power can be predicted using the statistics of the results. When the interference signal is transmitted from the interferer system to the actual environment, the received signal power is different each time due to the influence of the unpredictable conditions such as the direction of the antenna, the weather condition, and the location of the obstacles. The simulation using the MC method similarly calculates the radio interference power compared to the practical environment by stochastically approaching these unpredictable factors.

The purpose of a coexistence study is to identify and enable the compatibility between adjacent or co-channel systems through the interference analysis. If the level of interference power causes a problem for the victim system, then the coexistence of the systems is not guaranteed. In this case, there are several techniques that are taken to mitigate the radio interference power to ensure coexistence [11]–[13].

The simplest way is to increase the physical distance between the interferer and victim. As the distance between the two systems increases, the interference power is weakened [11]–[13]. This method can effectively reduce interference due to the exponentially increasing path loss. It is a suitable method for fixed systems but can be hard to apply for mobile systems with high mobility, unless the separation is defined to an operational regulation. If it is difficult to obtain the separation distance, the interference power can be suppressed through the frequency separation [11]–[13]. The receiver filter of the victim system receives the lower interference power due to the out-of-band emissions (OOBE) of the interferer system, because the power spectral density (PSD) level of the interferer system is lowered as the gap from the center frequency generally increases. However, this is accompanied by a waste of scarce frequency resources. Therefore, methods that maximize the interference mitigation effects with a minimum frequency separation should be applied.

Orthogonal frequency division multiplexing (OFDM) is applied as a general modulation method in various wireless communication systems. A waveform based on the OFDM carries informational data through a large number of subcarriers that are orthogonal to each other [14]. As shown in Fig. 1, these appear in the frequency domain in the form of an

overlapping narrowband spectra. The level of OOBE is relatively low, considering that all subcarriers are added, when compared to a single carrier signal with the same bandwidth. Despite the disadvantage of a high peak-to-average power ratio (PAPR), OFDM is advantageous in terms of frequency efficiency.

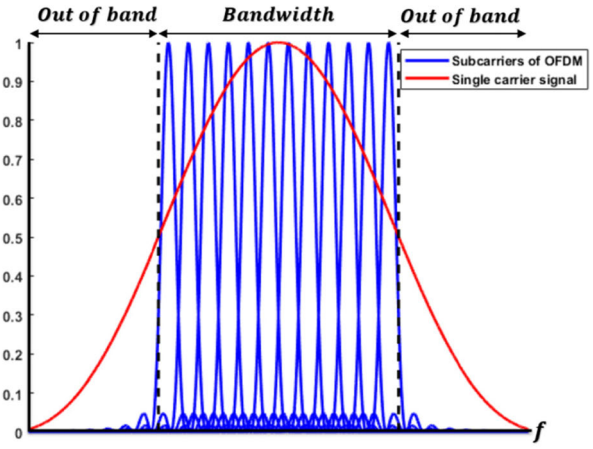

FIGURE 1. PSD of OFDM subcarriers and single carrier waveform.

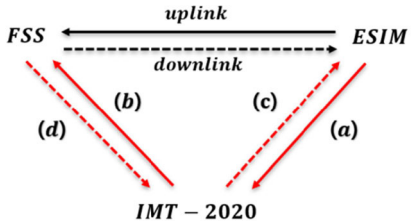

FIGURE 2. Interfering link.

B. RELATED WORKS AND CONTRIBUTIONS

In this study, the interference in the band adjacent to 27.5 GHz[1] is analyzed for the compatibility of ESIM and IMT-2020. As shown in Fig. 2, a total of four interfering links are present when the ESIM communicates with the FSS satellite. Interfering links (a) and (b) that occur during the uplink of the ESIM are indicated by solid arrows, and interfering links (c) and (d) occur during the downlink are indicated by dotted arrows. The interference by the links (c) and (d) is expected to be weak because the ESIM downlink service is considered in 17.7–19.7 GHz, so links (a) and (b) need to be considered. When the ESIM transmits a signal to the FSS satellite, the link (a) indicates that the IMT-2020 network is receiving it, which is radio interference. The link (b) is generated by communication between the base station (BS) and the user equipment (UE) in the IMT-2020 network, so the FSS satellite receive the radio interference from that. Several studies regarding link (b) have indicated that the co-channel interference from 5G systems to FSS satellites satisfies the protection criteria [15], [16]. The authors of [15] and [16] analyzed the aggregate interference from the IMT-2020 to the FSS satellite at an altitude of approximately 36000 km based on terrain altitude data and proved that the frequency sharing of the two systems is possible. Thus, the study of link (a) should be emphasized, which represents the interference from ESIM to IMT-2020.

Several studies regarding the interfering link (a) have been conducted [17]–[19]. The authors of [17] presented a minimum separation distance between the M-ESIM and IMT-2020 by applying the MCL method. The analysis assumed that the M-ESIM is located on the East and West Sea of South Korea, which communicates with the FSS satellite. As a result, the minimum distances between the two systems are 25 km for the East Sea and 8 km for the West Sea. The authors of [18] also conducted an analysis on the M-ESIM and suggested the separation distance by applying the MC method. The authors of [19] recently presented interference-to-noise ratio (I/N) results according to the guard band and the separation distance by applying various waveforms to the three types of ESIM. In summary, existing studies regarding the IMT-2020 receiving interference from ESIM did not consider the MC method or all forms of ESIM, to the best of our knowledge. In addition, a typical protection criterion I/N was only applied for accessing compatibility.

In contrast, both the MCL and MC methods were applied to simulate not only the worst, but also most practical interference effects for all types of ESIM including: M-ESIM, L-ESIM, and A-ESIM. For the MC based interference analysis, the multi-tier multi-cell IMT-2020 radio access network interfered by M-ESIM or L-ESIM was modeled, where the spatial and temporal changes in signal to interference plus noise ratio (SINR) of the IMT-2020 up-and down-link are accurately implemented using a universally recognized probability model. By leveraging this realistic model, the throughput loss as well as the I/N of IMT-2020 due to ESIM interference was simulated, followed by the quantification of the separation in distance and frequency for satisfying the desired excessing probability of I/N and throughput loss. Unlike a dichotomous approach using the fixed I/N criteria, the excessing probability-based protection enables more flexible and active system compatibility. Several elevation angles of the ESIM antenna are set to generalize the analysis results, which can be applied to various regions as well as a specific area.

To capture the realistic effects of the adjacent channel interference, the transmission spectrum of a commercial single carrier ESIM equipment was measured, and the frequency response of a practical receiver filter was modeled. Furthermore, two OFDM waveforms were adopted, CP-OFDM and windowed OFDM, for ESIM communication to suppress its OOBE and accordingly mitigate adjacent channel interference. A mathematical expression was derived for the frequency dependent rejection (FDR) of the two OFDM waveforms for the varying guard band, considering the practical receiver filter. The FDR equations of the two waveforms for 5G were first proposed in [20], although it assumed an

[1]Part of the results were published in recent work [19].

ideal rectangular-shaped frequency response of a receiver filter.

The remainder of this article is structured as follows. Sections II and III present the methodology of the IMT-2020 modeling and the interference scenarios, respectively. Section IV presents the analysis methodology and system parameters. In section V, the FDRs of the proposed OFDM waveforms are analyzed and the signal of the ESIMs is measured. Section VI presents the simulation parameters and results of the interference analysis, after which the conclusions are drawn in section VII.

II. IMT-2020 MODELING FOR COEXISTENCE STUDY BETWEEN 5G AND OTHER SYSTEMS

The IMT-2020 in this section is a heterogeneous network developed by the 3GPP Technical Specification Group (TSG) Radio Access Network (RAN) Working Group 4 (WG 4) [21]. This is a network that communicates with BSs and UEs based on 5G specification, which is essential for obtaining realistic interference analysis results.

There are three layout models: Macro urban (UMa), micro urban (UMi), and indoor. Among them, the UMi is most similar to the actual urban environment because the distribution density of the BSs and UEs is the highest and the antenna direction is not fixed. Therefore, the IMT-2020 network of the UMi was modeled.

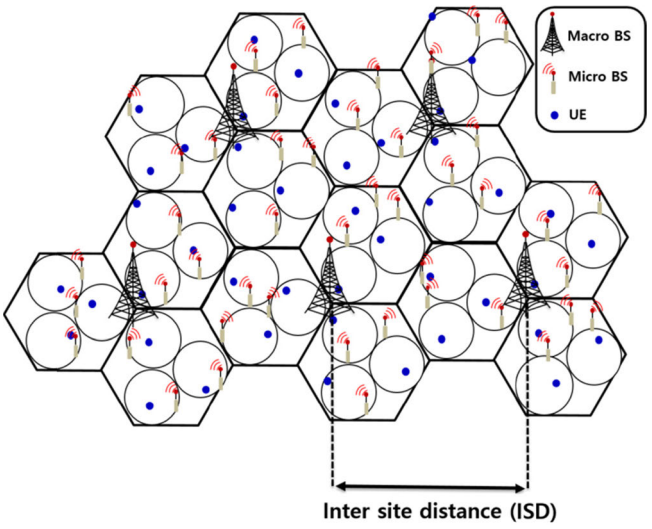

FIGURE 3. UMi layout model of IMT-2020.

As shown in Fig. 3, the UMi layout consists of hexagonal macro cells and circular micro cells. The three micro cells are inscribed in a macro cell. A macro BS is at the center of the three macro cells and covers them by a 3-sector antenna. A micro BS is located above the circumference of a micro cell and has a one sector antenna that points to the center of the circle. A UE has a 2-sector antenna, each covering 180°, and the distribution of that follows a uniform distribution for the area of a micro cell. Although this layout is apparently coexistent with the macro BS and the Micro BS, it is assumed that all UEs communicate with the micro BS in the 24.25–27.5 GHz range because the macro BS will be operated below 6 GHz for a wider coverage area, which is required to set the location of the micro cell. The macro BS and cell are necessary to set the location of the micro BS and cell.

A. PROPAGATION LOSS

The propagation loss model of the UMi layout in the IMT-2020 is roughly classified based on two factors; first, the Line-Of-Sight (LOS) probability which classifies LOS, and Non-Line-Of-Sight (NLOS). Here, LOS indicates that there is no obstacle between the transmitter and receiver, and the NLOS indicates an environment in which obstacles exist. The LOS probability is determined through the distance defined by Fig.4, and is given by the following:

$$P_{LOS} = \min\left(18/d_{2D}, 1\right)\left(1 - \exp\left(-d_{2D}/36\right)\right) + \exp\left(-d_{2D}/36\right), \quad (1)$$

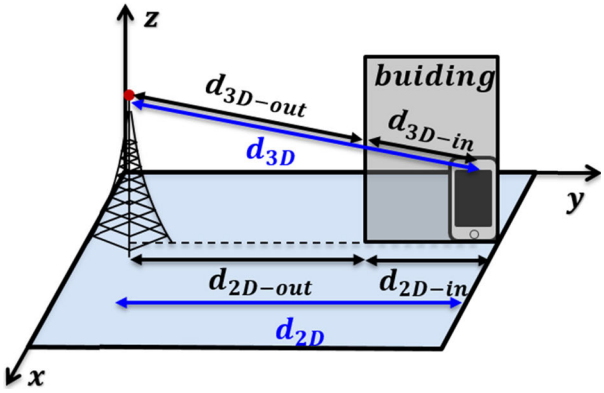

FIGURE 4. Definition of distance between BS and UE.

where d_{2D} is distance on the xy plane between the transmitter and receiver in m. Through the d_{3D}, which is the distance of the signal path, the path loss in the LOS environment is calculated as follows:

$$PL_{LOS} = 32.4 + 21\log_{10}(d_{3D}) + 20\log_{10}(f_c) + N\left(0, 4^2\right), \quad (2)$$

where f_c is the carrier frequency in GHz. The lognormal distribution of the last term in this equation reflects the shadow fading effect, with a mean of 0 dB and a standard deviation of 4 dB. The path loss in the NLOS environment is higher than that of the LOS due to obstacles and is expressed as follows:

$$PL_{NL} = 22.4 - 0.3\left(h_{UE} - 1.5\right) + 35.3\log_{10}\left(d_{3D}\right) + 21.3\log_{10}\left(f_c\right) + N\left(0, 7.82^2\right), \quad (3)$$

where h_{UE} is the antenna height of the UE and the shadow fading effect is reflected in the last term of this equation.

The second one determining path loss is the UE indoor ratio, which is the probability that the UE is distributed indoors and is set to 80% in the UMi layout model. The path loss is determined by (2) and (3), when the UE is

distributed outdoors. However, when the UE is distributed indoors, the path loss is given by the following:

$$PL = PL_b + PL_{in} + PL_{tw} + N\left(0, \sigma_P^2\right). \tag{4}$$

where PL_b is the basic outdoor path loss which can be calculated by substituting d_{2D-out} and d_{3D-out} instead of d_{2D} and d_{3D} in (1), (2) and (3); PL_{in} is the loss generated inside the building and calculated as $0.5 \cdot d_{2D-in}$ dB; and PL_{tw} is the building penetration loss through the external wall and is classified as a high/low loss model. Each ratio is 50%, which indicates that 50% of indoor UEs follow the high loss model and the remaining 50% follow the low loss model with a σ_P of 4.4 dB and 6.5 dB, respectively. Based on the above, the high loss and low loss model of the PL_{tw} are given by the following:

$$PL_{tw-high} = 5 - 10\log_{10}\left(0.7 \cdot 10^{-\text{L}_{\text{IRRglass}}/10} + 0.3 \cdot 10^{-\text{L}_{\text{concrete}}/10}\right), \tag{5}$$

$$PL_{tw-low} = 5 - 10\log_{10}\left(0.3 \cdot 10^{-\text{L}_{\text{glass}}/10} + 0.7 \cdot 10^{-\text{L}_{\text{concrete}}/10}\right), \tag{6}$$

where L is the material penetration loss, which depends on the material property of the building external wall in dB, L_{glass} is $2 + 0.2 \cdot f_c$, $\text{L}_{\text{IRRglass}}$ is $23 + 0.3 \cdot f_c$, and $\text{L}_{\text{concrete}}$ is $5 + 4 \cdot f_c$.

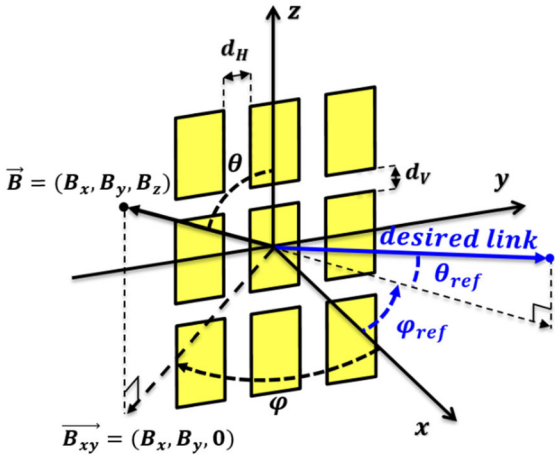

FIGURE 5. Definition of angles and parameters of the antenna array.

B. ANTENNA PATTERN MODEL OF IMT-2020

The 5G service employs 3D beamforming using a planar antenna array to compensate the high path loss in the mm Wave band. The IMT-2020 which we modeled, also implemented 3D beamforming with reference to the ITU-R Recommendation M.2101 [22]. The antenna gain of the IMT-2020 is calculated as the logarithmic sum of the element gain and array gain. The element pattern and array pattern are generated by a single element of the antenna and planar antenna array, respectively. Fig.5 presents the definition of the parameters for the IMT-2020 antenna pattern. The element pattern has the maximum gain at points $\theta = 90°$ and $\varphi = 0°$. The symbol θ (defined between 0° and 180°) and symbol φ (defined between −180° and 180°) are the elevation and azimuth angles of the signal direction, respectively. The elevation and azimuth angles at point B are given by the following:

$$\theta = \cos^{-1}\left(\frac{\vec{B} \cdot \hat{k}}{\left|\vec{B}\right|}\right), \tag{7}$$

$$\varphi = \begin{cases} \varphi_{temp} & \text{if } \hat{i} \times \overrightarrow{B_{xy}} \geq 0 \\ -\varphi_{temp} & \text{if } \hat{i} \times \overrightarrow{B_{xy}} < 0, \end{cases} \tag{8}$$

where

$$\varphi_{temp} = \cos^{-1}\left(\frac{\overrightarrow{B_{xy}} \cdot \hat{i}}{\left|\overrightarrow{B_{xy}}\right|}\right), \tag{9}$$

where $\hat{k} = (0, 0, 1)$ and $\hat{i} = (0, 0, 1)$ are unit vectors in the directions of the z-axis and x-axis, respectively. The element gain for θ and φ is given by the following:

$$E(\varphi, \theta) = E_{\max} - \min\{-[(E_H(\varphi) + E_V(\theta))], A_m\}, \tag{10}$$

where

$$E_H(\varphi) = -\min\left[12\left(\frac{\varphi}{\varphi_{3dB}}\right)^2, A_m\right], \tag{11}$$

$$E_V(\theta) = -\min\left[12\left(\frac{\theta - 90}{\theta_{3dB}}\right)^2, A_m\right], \tag{12}$$

where $E_{\max}$ is the maximum element gain in dBi, A_m is the front-to-back ratio, E_H is the horizontal radiation pattern, E_V is the vertical radiation pattern, θ_{3dB} is the vertical 3dB beam-width, and φ_{3dB} is the horizontal 3dB beam-width. Fig. 6 presents the 3D pattern of the element gain for the elevation and azimuth angles.

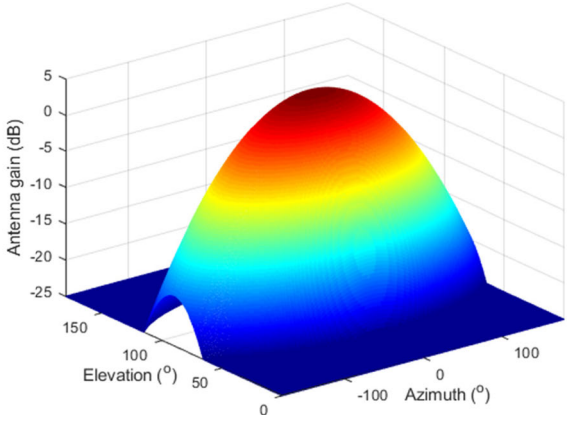

FIGURE 6. Element pattern of the BS.

The array pattern implements 3D beamforming, which increases the gain of the signal where it is desired. When the blue point in Fig. 5 is in the direction of the desired link,

the array gain at point B is given by the following:

$$A(\varphi,\theta) = 10\log_{10}\left(\left|\sum_{m=1}^{N_H}\sum_{n=1}^{N_V} w_{n,m}\cdot v_{n,m}\right|^2\right), \quad (13)$$

where

$$v_{n,m} = \exp\left(\sqrt{-1}\cdot 2\pi\left((n-1)\cdot\frac{d_V}{\lambda}\cdot\cos\theta + (m-1)\cdot\frac{d_H}{\lambda}\cdot\sin\theta\cdot\sin\varphi\right)\right), \quad (14)$$

$$w_{n,m} = \frac{1}{\sqrt{N_H N_V}}\exp\left(\sqrt{-1}\cdot 2\pi\left((n-1)\cdot\frac{d_V}{\lambda}\cdot\sin(90^\circ-\theta_{ref}) + (m-1)\cdot\frac{d_H}{\lambda}\cdot\cos(90^\circ-\theta_{ref})\cdot\sin\varphi_{ref}\right)\right), \quad (15)$$

where v is the superposition vector, w is the weighting vector, N_H is the number of horizontal antenna arrays, N_V is the number of vertical antenna arrays, d_H/λ is the horizontal radiating element spacing, d_V/λ is the vertical radiating element spacing, φ_{ref} is the azimuth angle of the desired link, and φ_{ref} is the elevation angle of the desired link. Fig. 7 presents the 3D pattern for the elevation and azimuth angles of the antenna gain of the IMT-2020 expressed by the logarithmic sum of the element and array pattern. When the desired direction is the point where the elevation angle is 90° and the azimuth angle is 0°, the difference in antenna gain from other points is significantly greater than the element pattern.

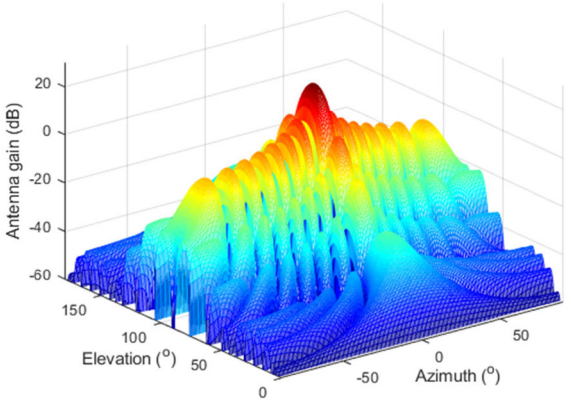

FIGURE 7. Composite pattern of the BS.

C. MODELLING THE IMT-2020 NETWORK

As shown in Fig. 8 (a), six virtual clusters are distributed around the main network to solve the edge effects, that is, the interference between the IMT-2020 terminals becomes asymmetric at the network edge and the center [22]; it is called a wrap-around method. In order to implement a communication environment in the network, the BS and the UE are paired 1 to 1 through the coupling loss. Each UE is connected to the one with the minimum coupling loss of all BSs. The coupling loss from the i-th UE to the j-th BS is as follows:

$$CL_{i,j} = PL_{i,j} - E_{BS\_i,j} - E_{UE\_i,j} \quad (16)$$

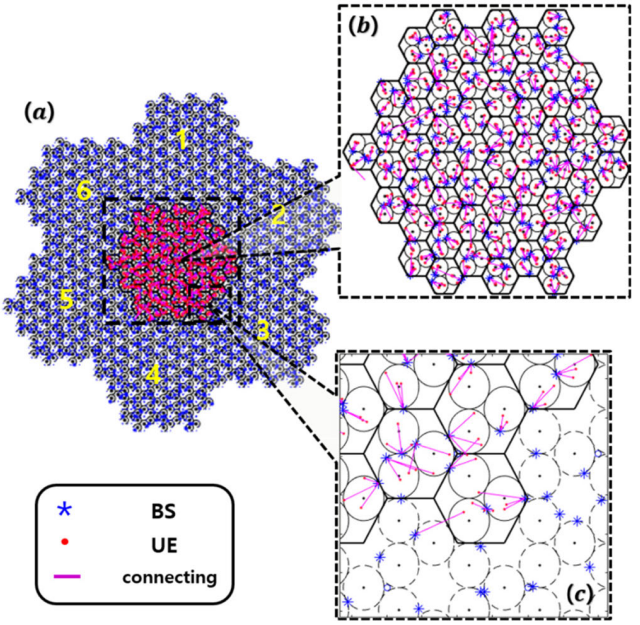

FIGURE 8. (a) Wrap-around methodology, (b) IMT-2020 network, (c) Connecting between BSs and UEs.

where PL is the path loss, E_{BS} is the element gain of the BS, and E_{UE} is the element gain of UE. Fig. 8 (b) and (c) indicates that a single BS is connected to multiple UEs, but assumes that it communicates with a single UE at a time through a round robin schedule.

After that, the beamforming is performed for the connected 5G terminal in each pair, and the inter-cell interference (ICI) is generated by the transmit signal. Here, allocations of downlinks (from the the BS to UE) and uplinks (from the UE to the BS) in the network are distributed by time through the time division duplexing (TDD). It is assumed that all downlinks and uplinks in the TDD network are performed simultaneously through synchronization, respectively. Therefore, the UEs receive interference for the downlink and the BSs receive interference for the uplink. The SINR is calculated to evaluate the communication performance in the network considering only the ICI. The received SINR of the UEs are managed in the downlink, and the j-th BS and i-th UE are assumed to be connected. The downlink SINR is given as follows:

$$SINR_{ICI\_i} = S_i/\left(I_{ICI\_i} + N\right), \quad (17)$$

where

$$S_i\,[dBm] = Pt_j + A_{BS\_i,j} + A_{UE\_i,j} - CL_{i,j}, \quad (18)$$

$$I_{ICI\_i}\,[dBm] = \sum_{k\neq j}\left(Pt_k + A_{BS\_i,k} + A_{UE\_i,k} - CL_{i,k}\right), \quad (19)$$

$$N\,[dBm] = -174 + 10\log_{10}(B_r) + NF, \quad (20)$$

where S_i is the signal power of the desired link from the j-th BS to the i-th UE, I_{ICI_i} is the power of ICI from the k-th BS to the i-th UE, N is the noise power of the receiver using the Boltzmann constant and ordinary temperature in the absolute

scale, Pt is the transmit power of the BS in dBm, A_{BS} is the array gain of the BS in dBi, A_{UE} is the array gain of the UE in dBi, B_r is the bandwidth of the UE in Hz, and NF is the noise figure in dB. In the uplink, i becomes the index of the BS, and j and k become the index of the UE. The uplink SINR can be calculated like the downlink SINR. In IMT-2020 uplink, the BSs receive the interference of the UEs distributed inside other micro cells through the same path loss given in (4). Note, the transmission power of all base stations is the same whereas the transmit power of each UE can be different by the power control indicated in ITU-R M.2101 [22]. Chapters 7, 8, and 9 of [23] evaluate the relative performance degradation of networks by adjacent channel interference ratio (ACIR). According to [23], small scale fading is not considered to reduce simulation complexity. The SINR in this study is also used as a measure to evaluate performance degradation by other systems in adjacent bands, so small scale fading is omitted in the calculation process.

III. INTERFERENCE SCENARIO

This section presents scenarios to analyze the interference from the ESIM to 5G. Because ESIM is classified into three types according to the operation environment, the propagation loss model and additional loss applied to each are different. Therefore, a total of three interference scenarios are constructed and the interference analysis with 5G is performed. In this study, multiple ESIMs are not considered because only one ESIM is operated on one channel at a time by the time division multiple access (TDMA) [24]. In other words, even if multiple ESIMs are operated, only one ESIM at a time will have an interference effect.

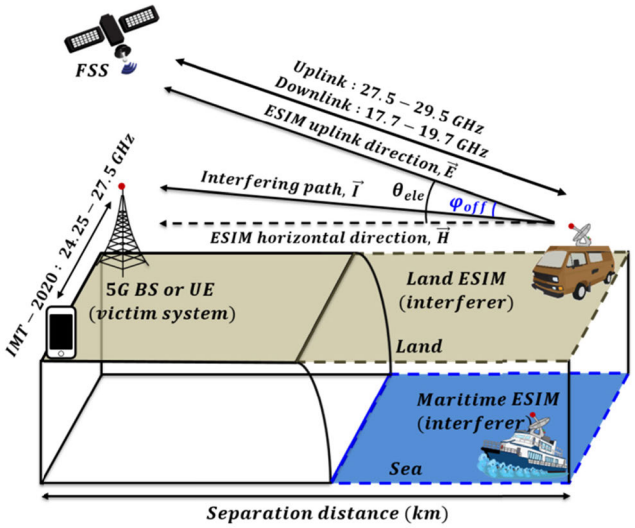

FIGURE 9. MCL scenario of M-ESIM and L-ESIM.

A. MARITIME ESIM OR LAND ESIM

When the interferer type is M-ESIM or L-ESIM, the MCL and MC is applied to the interference analysis. First, in MCL analysis, as shown in Fig. 9, M-ESIM and L-ESIM are located on land and sea, respectively, and a single 5G BS or a single UE is distributed on land. The antenna of the ESIM points directly to the FSS satellite along the uplink path of the ESIM. The θ_{ele} denotes the elevation angle of the FSS satellite (which is referred to as the elevation angle of the ESIM antenna in this study), which is formed by the uplink path with the horizontal direction of the ESIM. The interfering path ($\vec{I}$) is from the ESIM to the 5G terminals, and forms an off-axis angle (φ_{off}) with the uplink path of the ESIM. Fig. 10 presents the mapping of the interference scenario to the Cartesian coordinate. When the main beam of the ESIM faces the FSS satellite, the effective isotropic radiated power (EIRP) of the ESIM, which IMT-2020 receives, is determined by the φ_{off}. The angle φ_{off} of n-th interfering path is as follows:

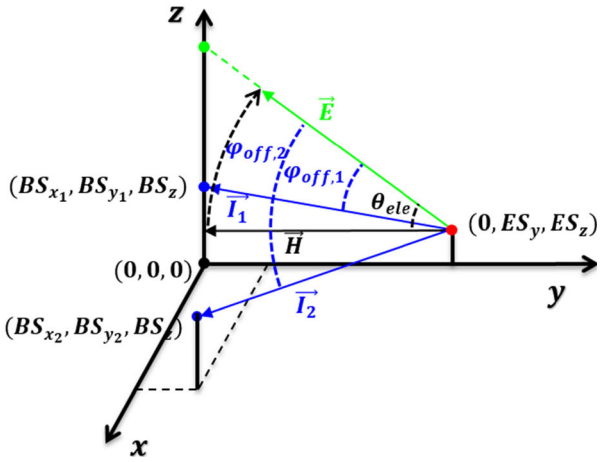

FIGURE 10. Mapping the ESIM and the BS to 3D space.

$$\varphi_{off,n} = \cos^{-1}\left(\frac{\vec{E}\cdot\vec{I_n}}{\left|\vec{E}\right|\left|\vec{I_n}\right|}\right), \tag{21}$$

where $\vec{I_n}$ is the vector of the n-th interfering path, and $\vec{E}$ is the vector of the ESIM uplink path. These can be represented in Fig. 10 as follows:

$$\vec{I_n} = (BS_{x_n}, BS_{y_n} - ES_y, BS_z - ES_z) \tag{22}$$

$$\vec{E} = R_x(-\theta_{ele})\,\vec{H}, \tag{23}$$

where $\vec{H}$ is the vector of the ESIM horizontal direction, and R_x is the 3 dimensional rotation matrix about the x-axis. These are expressed as follows:

$$\vec{H} = (0, -ES_y, 0) \tag{24}$$

$$R_x(\alpha) = \begin{bmatrix} 1 & 0 & 0 \\ 0 & \cos\alpha & -\sin\alpha \\ 0 & \sin\alpha & \cos\alpha \end{bmatrix}, \tag{25}$$

As shown in Fig. 9, it is assumed that the FSS satellite, ESIM, and victim systems are located on the same horizontal line, thus they face each other in the azimuth direction between the ESIM and the victim systems. Considering the BS antenna, the element gain is determined by applying a

downwards tilt to direct the UE below the BS. However, assuming that beamforming is deployed in the direction of the ESIM, the maximum value of the array gain is applied. The UE antenna direction is relatively free, thus both the element and array gains are set to the maximum value in consideration of directly pointing to the ESIM.

In the MC method, the single IMT station of Fig. 9 is replaced by the IMT-2020 network presented in Fig. 8. The antenna direction of the ESIM is the same as that of the MCL, but the antenna direction of the BS and the UE in the IMT-2020 is directed to the communicating UE and BS, respectively, not to the ESIM antenna. Therefore, both ESIM and IMT antenna gains vary depending on their location.

The MC is applied when the M-ESIM and L-ESIM are located outside the IMT-2020 network. In the case of L-ESIM, the possibility of being located inside the IMT-2020 should also be considered. However, because the ESIM will be operated in areas where wireless communication and networks are not possible, the operation of the L-ESIM inside the IMT-2020 does not meet the purpose of the ESIM. However, this study analyzed the case where L-ESIM is located inside the IMT-2020 to present various cases to users.

B. AERONAUTICAL ESIM

A-ESIM is mounted and operated on the aircraft. In this study, interference analysis is performed when the aircraft is operating in the air, and the minimum altitude that can coexist with the IMT-2020 is derived. The same interference scenario is considered in [25], where a constant FDR value independent of the guard band is adopted. In contrast, the FDRs of three waveforms proposed in Section V are considered in this study.

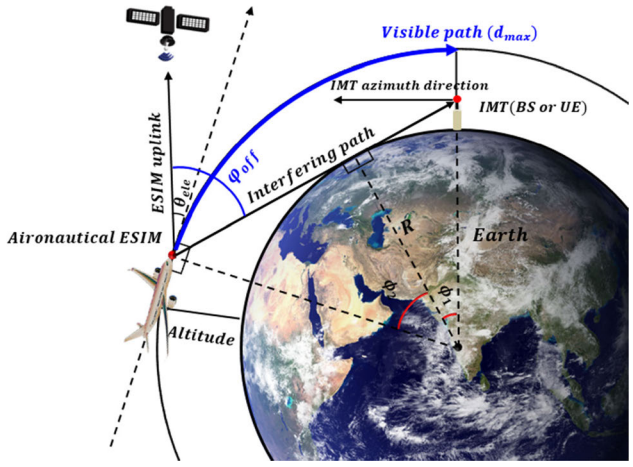

FIGURE 11. MCL scenario of A-ESIM.

As shown in Fig. 11, A-ESIM is assumed to fly at a constant altitude and elevation angle. At this time, considering the curvature of the circumference of the Earth, the maximum distance that the IMT-2020 can observe for the aircraft can be calculated. This is called the maximum visible path and is expressed as follows:

$$d_{\max} = (R + Al) \cdot (\phi_1 + \phi_2), \tag{26}$$

where

$$\phi_1 = \tan^{-1}\left(\frac{\sqrt{(R+h)^2 - R^2}}{R}\right), \tag{27}$$

$$\phi_2 = \tan^{-1}\left(\frac{\sqrt{(R+Al)^2 - R^2}}{R}\right), \tag{28}$$

where R is the radius of the Earth (m), Al is the altitude of the A-ESIM (m), and h is the antenna height of the IMT-2020 system (m). The maximum visible path should be analyzed by setting the path of the $2d_{\max}$ range, considered when passing the IMT-2020 system. However, when the A-ESIM deviates from the path in the direction of $d_{\max}$ in Fig. 11, the interference power will be significantly small because it is opposite to the direction of the IMT-2020 antenna. Thus, only the $d_{\max}$ of the path where the IMT-2020 antenna direction and the ESIM antenna direction face each other is considered and analyzed. This scenario analyzes a target with a minimum altitude that does not exceed the interference criterion by setting a certain altitude and calculating the interference power within the $d_{\max}$. Fig. 12 presents the maximum visible path according to the altitude of the A-ESIM [25].

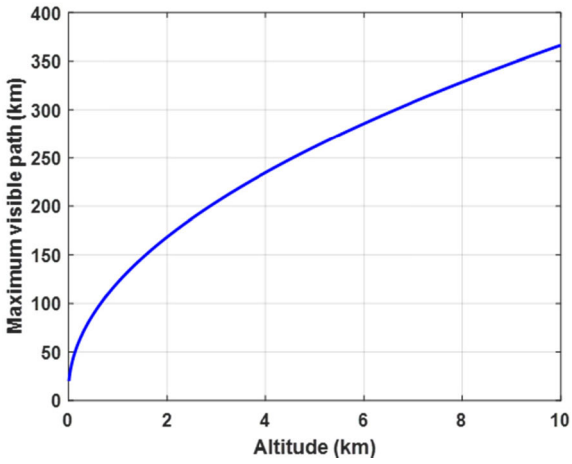

FIGURE 12. Maximum visible path according to altitude of A-ESIM.

Similar to the M-ESIM and L-ESIM scenarios, the received antenna gain of the BS calculates the element gain according to the position of the A-ESIM considering the downward tilt of the antenna, and applies the maximum value to the array gain. The UE also assumes the maximum of the element and array gains, as in the other two ESIM scenarios. Considering the A-ESIM, only the MCL analysis is performed, not the MC analysis.

IV. INTERFERENCE ANALYSIS METHODOLOGY

A. INTERFERENCE TO NOISE RATIO

I/N is the most used indicator in interference analysis. This can be calculated by simply dividing the interference power

by the noise power of the victim system. The noise power N of the victim system is previously referred to (20). The adjacent channel interference (ACI) from the ESIM is calculated as follows:

$$I_{ACI}\,[dBm] = E_{ESIM}\left(\phi_{off}\right) + G_r - L_p - L_r - \mathrm{FDR}, \quad (29)$$

where E_{ESIM} is the EIRP of ESIM according to the off-axis angle, G_{r} is the received antenna gain of the victim system, L_{p} is the propagation loss, L_{r} is the additional loss occurring in the ESIM and IMT-2020 system, and FDR is the frequency dependent rejection.

EIRP is the sum of the output power and the antenna gain. The EIRP level is expressed as follows:

$$E_{ESIM}\left(\varphi_{off}\right)\,[dBW/40kHz] = \begin{cases} 19 - 25\log_{10}\varphi_{off} & \text{if } 2^\circ \le \varphi_{off} \le 7^\circ \\ -2 & \text{if } 7^\circ \le \varphi_{off} \le 9.2^\circ \\ 22 - 25\log_{10}\varphi_{off} & \text{if } 9.2^\circ \le \varphi_{off} \le 48^\circ \\ -10 & \text{if } 48^\circ < \varphi_{off} \le 180^\circ, \end{cases} \quad (30)$$

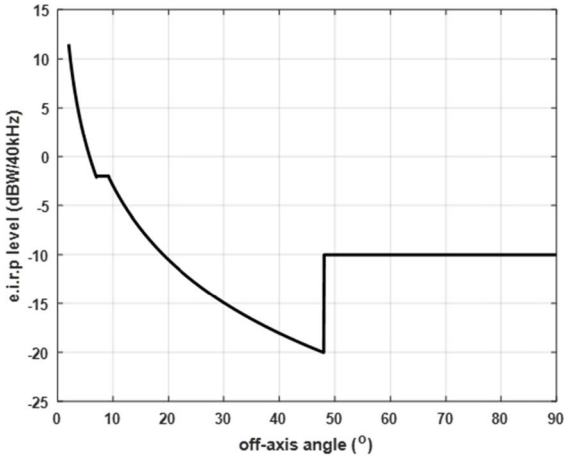

FIGURE 13. The EIRP level of ESIM.

Fig. 13 presents the EIRP level of the ESIM, and it can be confirmed that the level is saturated at an off-axis angle of 48°. The pattern is referred to ITU-R Recommendation S.524-9 [26]. The EIRP level introduced in this document is the limit of the EIRP level according to the angle, considering the possibility that the earth station communicating with the FSS satellite will interfere with other FSS satellites. Therefore, Fig. 13 is intended to limit the output of the earth station, so that some discontinuous patterns appear.

FDR is determined by the channel selectivity of the receiver and the unwanted emission of the transmitter, and is calculated as follows [27]:

$$\mathrm{FDR} = 10\log_{10}\left(\frac{\int_{-\infty}^{\infty}\Phi(f)df}{\int_{-\infty}^{\infty}\Phi(f)\Psi(f-\Delta f)df}\right), \quad (31)$$

where $\Phi(f)$ is the PSD of interfering signal, $\Psi(f)$ is the normalized frequency response of the receiver, and Δf is the frequency offset. As shown in Fig. 14, the guard band is obtained as follows through the frequency offset:

$$GB = \Delta f - \frac{W_T}{2} - \frac{W_R}{2}, \quad (32)$$

where W_T is the channel bandwidth of the transmitter, and W_R is the channel bandwidth of the receiver.

TABLE 1. Parameters of throughput loss.

Parameter	Downlink	Uplink	Unit
Attenuation, α	0.6	0.4	
Minimum SINR	-10	-10	dB
Maximum SINR	30	22	dB

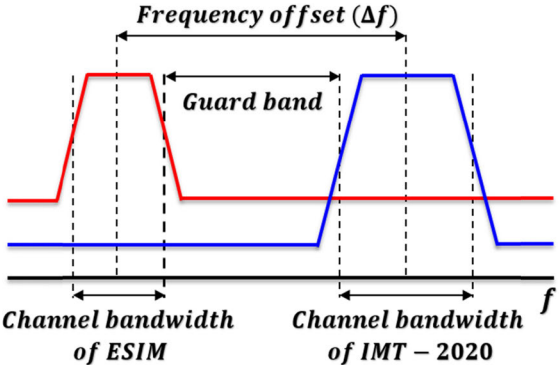

FIGURE 14. Definition of frequency offset and guard band.

The ACI from the ESIM causes the victim system to fail due to the interference power above a certain value. Thus, acceptable interference is set to limit the reception of the interference power beyond that. The maximum acceptable interference is calculated by the I/N threshold as follows:

$$I_{th} = I/N_{th} + N, \quad (33)$$

where N is the noise power of victim system and is expressed in (20). In [9], the I/N threshold of the IMT-2020 system is set to -6 dB. The compatibility is confirmed through the minimum separation distance and the minimum guard band that satisfies $I_{th} \le I_{ACI}$ from the interferer system.

B. THROUGHPUT LOSS

Throughput loss is an indicator of the extent to which the communication performance is degraded by the interferer system. This analysis deals with the throughput reduced by the ACI of the ESIM in the IMT-2020 network, and the throughput loss is expressed as follows [21]:

$$Throughput\ loss = 1 - (Throughput_{ACI}/Throughput_{ICI}), \quad (34)$$

where $Throughput_{ICI}$ is the throughput of the IMT-2020 system in the network, and $Throughput_{ACI}$ is the throughput when receiving ACI in the IMT-2020 network. The two types

of throughputs are calculated by applying the attenuation in Table 1 to Shannon capacity, and expressed as follows:

$$Throughput_{ICI} = \log_2(1 + \alpha SINR_{ICI}), \quad (35)$$

$$Throughput_{ACI} = \log_2(1 + \alpha SINR_{ACI}), \quad (36)$$

The $SINR_{ACI}$ is the SINR of the IMT-2020 system in the network when receiving the ACI from the ESIM, and is expressed as follows:

$$SINR_{ACI} = S/(I_{ICI} + I_{ACI} + N) \quad (37)$$

The Throughput loss is a probability value and has a value between 0 and 1. The closer the throughput loss is to 0, the smaller the performance degradation by the ACI. Based on Table 1, the throughput loss is 1 when the $SINR_{ACI}$ is less than the minimum SINR, and 0 when it is greater than the maximum SINR [21].

C. PROPAGATION LOSS

The environment in which radio waves are transmitted is set differently for each interference scenario. Therefore, the propagation loss model according to each scenario should also be applied differently. The propagation loss has the largest effect on the interference power, thus applying reliable models is essential for analyzing an accurate interference.

Considering setting M-ESIM and L-ESIM as interferers, the propagation model implemented with reference to ITU-R Recommendation P.452-16 [28] is used. This is applicable when both the interferer and the victim systems are on the surface of the earth and the frequency band is 100 MHz–50 GHz. In addition, it reflects all propagation phenomena occurring in the terrestrial radio waves. These propagation phenomena are largely divided into long term and short-term propagation.

The long-term propagation phenomenon reflects the effects of line-of-sight, diffraction, and tropospheric scatter, and the short-term indicates unusual propagation in a short period of time such as during rain fall and certain weather events. This phenomenon reflects the line-of-sight with multipath enhancements, hydrometeor scatter, elevated layer reflection/refraction, and ducting. The user can set the time percentage in the range of $0.001\% \leq p \leq 50\%$ to reflect the long-term and short-term propagation phenomena. Usually, the time percentage of the long-term propagation is 20% and that of the short-term is 1% [29], [30]. In addition, the P.452 model is suitable for analyzing the M-2SIM and L-ESIM because it is possible to classify the environment in which the radio waves are transmitted from inland, sea, and coastal land. In this study, only the 20% long-term propagation phenomenon was considered, and the zone type for the M-ESIM and L-ESIM scenarios was set to sea and inland, respectively.

The A-ESIM is not suitable for applying the P.452 model because it is an aeronautical system, unlike the M-ESIM and L-ESIM. Therefore, in the A-ESIM scenario, free space loss which is traditionally used is applied to the analysis of interference between the ground systems and aeronautical systems, per the following equation [31]:

$$L_{free} = 20\log_{10}\left(\frac{4\pi df}{c}\right), \quad (38)$$

where d is the distance between the two systems (m), f is the frequency (Hz), and c is speed of light (m/s). In addition, because the A-ESIM is mounted on an aircraft, signal attenuation occurs by the fuselage of the aircraft. Fuselage loss is based on the model presented in ITU-R Recommendation M.2221 and is presented in Fig. 15. This pattern is a model that measures the attenuation of a signal by installing an antenna on a cylinder similar to the Boeing 737 fuselage at 14.2 GHz. Therefore, it may not be appropriate to apply this study considering the 27.5 GHz band. However, because the signal in the 27.5 GHz band has a shorter wavelength than the 14.2 GHz band, the loss due to the fuselage is greater, thus this model is applied to this study assuming the worst interference situation.

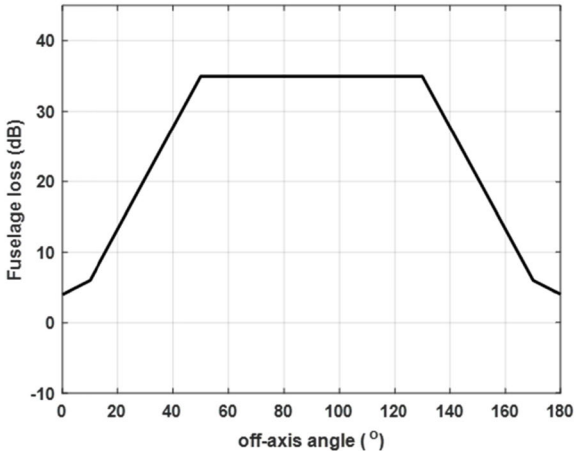

FIGURE 15. Fuselage loss according to off-axis angle.

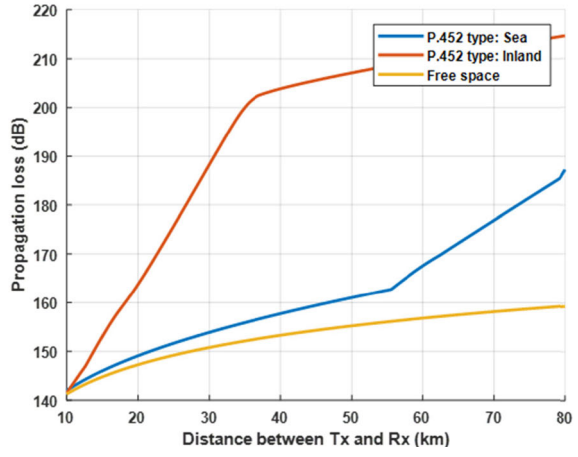

FIGURE 16. Propagation loss profile depends on environments.

Fig. 16 presents the profile of the propagation loss according to the separation distance by sea, inland, and free space, which are the distribution environments of M-ESIM,

L-ESIM, and A-ESIM, respectively. When the separation distance is the same, the propagation loss in the free space was the smallest, and that in the land environment was the highest.

V. ESIM WAVEFORMS FOR INTERFERENCE MITIGATION

A transmitting waveform with a low OOBE increases the FDR and accordingly, reduces the adjacent channel interference. The FDR in this study is calculated using three signals. First, the actual M-ESIM measurement waveform shown in Fig. 17 is used. Fig. 17 presents a single carrier with a bandwidth of 1 MHz on a 32 MHz channel. This waveform is a signal that can be extended to a bandwidth of up to 7 MHz according to the needs of the user.

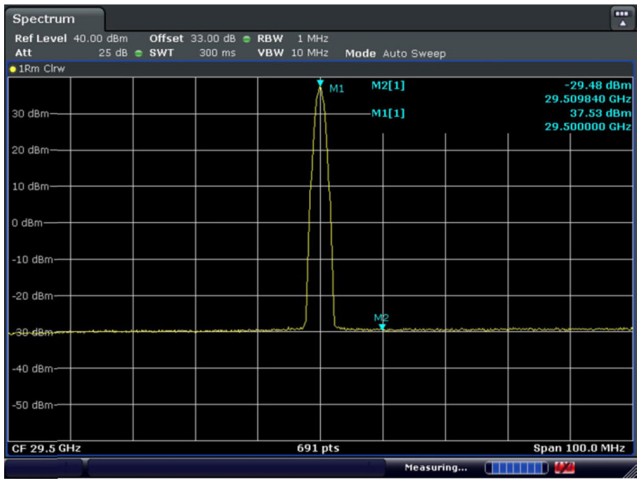

FIGURE 17. Measured frequency domain waveform of ESIM.

The other two signals implemented the OFDM. This study proposes two waveforms of the ESIM using the cyclic prefix (CP)-OFDM and the windowed-OFDM; it derives the FDR according to the type of signal through a practical frequency response of the receiver modeling.

A. FREQUENCY DEPENDENT REJECTION OF MEASURED SIGNAL AND FREQUENCY RESPONSE OF RECEIVER

The measured frequency-domain waveform shown in Fig. 17 has a carrier bandwidth of 1 MHz. However, according to [5], the ESIM has various channel bandwidths of up to 100 MHz. The channel of the measured waveform is extended to 90 MHz, and the carrier bandwidth is extended to approximately 81 MHz which is 90% of the channel bandwidth. The minimum level of unwanted emissions due to expansion is assumed to be set at −67 dB lower than a peak level, as shown in Fig 17.

In calculating the FDR, the value is determined by the PSD of the transmitted signal and the frequency response of the receiver. The ideal frequency response of the receiver is a flat response over the entire reception channel bandwidth. However, in this study, to implement the practical frequency response of the receiver, it is modeled as in Fig. 18 and can

TABLE 2. Parameters of receiver filter.

Parameter	Value	Symbol	Unit
Channel bandwidth	200	W_R	MHz
Flat response bandwidth	194	W_f	MHz
Transition bandwidth	394	W_t	MHz
Stopband attenuation	-100	b	dB

be expressed as follows:

$$\Psi(f)[\mathrm{dB}]=\begin{cases} b & \text{if } |f| \geq \frac{w_t}{2} \\ 0, & \text{if } |f| \leq \frac{w_f}{2} \\ \left(\frac{2b}{(w_f-w_t)}\right)\left(f+\frac{w_f}{2}\right) & \text{if } -\frac{w_t}{2} \\ & <f<-\frac{w_f}{2} \\ \left(\frac{2b}{(w_t-w_f)}\right)\left(f-\frac{w_f}{2}\right) & \text{if } \frac{w_f}{2}<f<\frac{w_t}{2}, \end{cases} \tag{39}$$

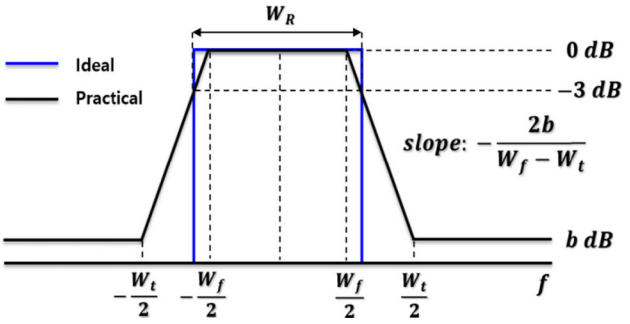

FIGURE 18. Frequency response of ideal and practical receiving filter.

where W_f is the bandwidth of the flat response, W_t is the transition bandwidth, and W_R is the bandwidth of the receiver channel. Table 2 presents the parameters of the frequency response of the receiver. These values are set based on [32], and the programs are provided for general users to easily implement various types of filters. These values are set with a 10^{th} order bandpass filter.

B. POWER SPECTRAL DENSITY OF CP-OFDM AND WI-NDOWED OFDM

OFDM causes an inter-symbol interference and an inter-channel interference when the orthogonality between the subcarriers is broken. To solve this problem, guard intervals between data symbols are placed to perform cyclic prefix [33]. This is called CP-OFDM for which the baseband signal is expressed as follows:

$$s(t)=\sum_{n=-\infty}^{\infty}\sum_{k=0}^{N-1}c_{n,k}p\left(t-n\left(T_s+T_g\right)\right)e^{-j2\pi k\frac{1}{N}\left(T_s+T_g\right)} \tag{40}$$

where N is the number of subcarriers, $c_{n,k}$ is a data symbol modulated on the k-th subcarrier of the n-th OFDM symbol, $p(t)$ is a pulse shaping window, T_s is the length of the data symbol, and T_g is a guard interval.

When each subcarrier is statistically independent and mutually orthogonal, the PSD of the OFDM to which an arbitrary pulse shaping window is applied is as follows [34], [35]:

$$\Phi(f) = \frac{P_s}{T_{total}} \sum_{k=0}^{N-1} \left| P\left(f - \frac{k}{T_s}\right) \right|^2, \tag{41}$$

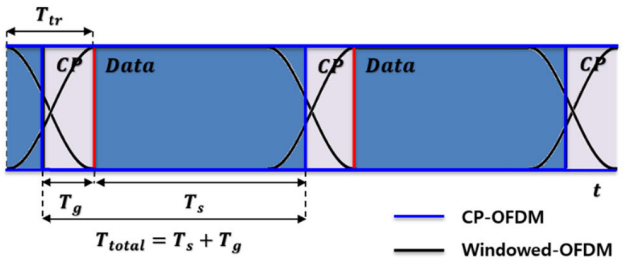

FIGURE 19. CP-OFDM and windowed-OFDM waveform in time-domain of ESIM.

where P_s is the power of a subcarrier, $P(f)$ is the Fourier transform of the pulse shaping window, and $T_{total} = T_s + T_g$ is total symbol duration. As indicated by the blue line in Fig. 19, the CP-OFDM subcarrier uses a rectangular pulse shaping window in the time domain expressed as follows:

$$p_{CP}(t) = \prod\left(\frac{t}{T_{total}}\right) = \begin{cases} 0 & \text{if } t > \left|\frac{T_{total}}{2}\right| \\ 1 & \text{if } t \le \left|\frac{T_{total}}{2}\right|, \end{cases} \tag{42}$$

The Fourier transform of (42) is expressed as follows:

$$P_{CP}(f) = T_{total} \cdot \mathrm{sinc}\left(T_{total} f\right), \tag{43}$$

where the function is defined as $\mathrm{sinc}(x) = \sin(x\pi)/x\pi$. Substituting (43) into (41) gives the PSD of CP-OFDM as follows:

$$\Phi_{CP}(f) = P_s T_{total} \sum_{k=0}^{N-1} \left\{ \mathrm{sinc}\left[\left(f - \frac{k}{T_s}\right) T_{total}\right] \right\}^2 \tag{44}$$

The windowed-OFDM is a proposed technique to improve the spectral efficiency. This can reduce the OOBE because it uses a smoother window than the rectangular pulse shaping window used in the CP-OFDM. Due to these advantages, in this study, a window using a raised cosine function in the time domain was applied as follows:

$$p_{WO}(t) = \begin{cases} 1 & \text{if } |t| \le \dfrac{(T_{total} - T_{tr})}{2} \\ \dfrac{1}{2}\left(1 + \cos\left(\dfrac{\pi\left(|t| - (T_{total} - T_{tr})/2\right)}{T_{tr}}\right)\right) & \text{if } \dfrac{(T_{total} - T_{tr})}{2} \le |t| < \dfrac{T_w}{2} \\ 0 & \text{if } \dfrac{T_w}{2} \le |t|, \end{cases} \tag{45}$$

where T_{tr} is the transition time, and $T_w = T_{total} + T_{tr}$ is the duration of the window. As indicated by the black line in Fig. 19, it has a smooth curved shape during the transition time. The Fourier transform of (45) is expressed as follows:

$$P_{WO}(f) = \frac{T_{total}\,\mathrm{sinc}\left(T_{total} f\right) \cdot \cos\left(\pi T_{tr} f\right)}{1 - 4T_{tr}^2 f^2} \tag{46}$$

Substituting (46) into (41) provides the PSD of the windowed-OFDM as follows:

$$\Phi_{WO}(f) = P_s T_{total} \sum_{k=0}^{N-1} \left\{ \mathrm{sinc}\left[\left(f - \frac{k}{T_s}\right) T_{total}\right] \times \frac{\cos\left(\pi T_{tr}\left(f - \frac{k}{T_s}\right)\right)}{1 - 4T_{tr}^2\left(f - \frac{k}{T_s}\right)^2} \right\}^2 \tag{47}$$

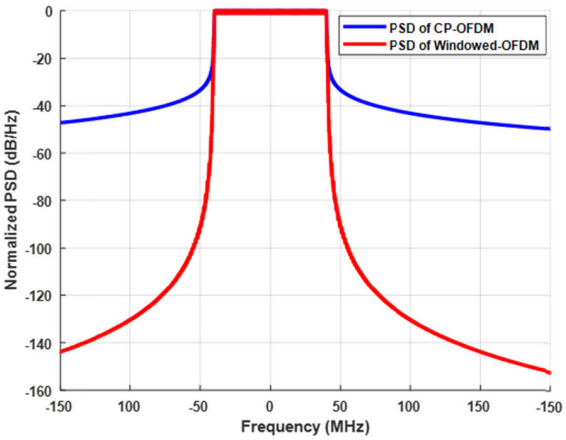

FIGURE 20. PSD of CP-OFDM and windowed-OFDM.

Fig. 20 presents the PSD of CP-OFDM and windowed-OFDM by applying the parameters in Table 3. The OOBE is suppressed in the windowed-OFDM using a smooth pulse shaping window. The OFDM parameters in Table 3 were set with reference to 5G numerology [36], which is a typical system using OFDM waveforms.

Substituting the derived PSD of OFDM waveforms and (39) into (31), the FDR is obtained by the following equation:

$$\begin{aligned} \mathrm{FDR} &= P_t - 10\log_{10}\left(\int_{-\infty}^{\infty} \Phi(f)\Psi(f - \Delta f)df\right) \\ &= P_t - 10\log_{10}\left(\int_{-\infty}^{\Delta f - \frac{w_t}{2}} \Phi(f) \cdot 10^{\frac{b}{10}} df \right. \\ &\quad + \int_{\Delta f - \frac{w_t}{2}}^{\Delta f - \frac{w_y}{2}} \Phi(f) \cdot 10^{\left(\left(\frac{2b}{w_y - w_s}\right)\left(f - \Delta f + \frac{w_y}{2}\right)\right)} df \\ &\quad \left. + \int_{\Delta f - \frac{w_y}{2}}^{\Delta f + \frac{w_y}{2}} \Phi(f) df \right) \end{aligned}$$

$$+\int_{\Delta f+\frac{w_v}{2}}^{\Delta f+\frac{w_t}{2}}\Phi(f)\cdot 10^{\left(\left(\frac{2b}{w_t-w_v}\right)\left(f-\Delta f-\frac{w_v}{2}\right)\right)}df$$
$$+\int_{\Delta f+\frac{w_t}{2}}^{\infty}\Phi(f)\cdot 10^{\frac{b}{10}}df\Bigg),$$
$$\text{where } P_t=\int_{-\infty}^{\infty}\Phi(f)df, \tag{48}$$

TABLE 3. Parameters of OFDM signal.

Parameter	Value	Symbol	Unit
Channel bandwidth	90	N/A	MHz
Signal bandwidth	80.6	N/A	MHz
Output power	37	P_t	dBm
Number of subcarriers	672	N	N/A
Data symbol duration	8.33	T_s	μs
Subcarrier spacing	120	$1/T_s$	kHz
Guard interval	0.57	T_g	μs
Transition time	0.8228	T_{tr}	μs

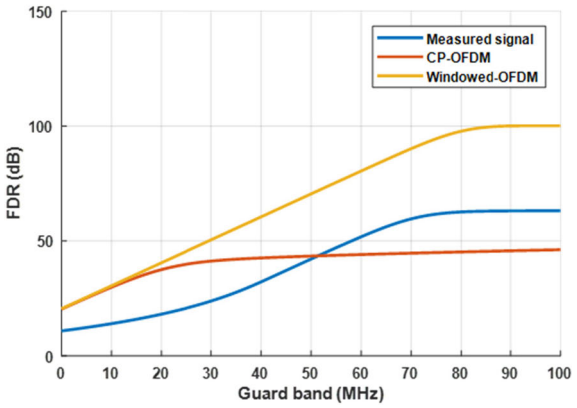

FIGURE 21. FDR of measured signal, CP-OFDM and windowed-OFDM.

Although the FDR expressions are not closed-form, they are simple to calculate using the numerical computing software. Figure 21 presents the FDR of three types of signals according to the guard bands obtained based on the equations and Tables 2 and 3. Up to approximately 50 MHz, the guard band has a high FDR value in the order of windowed-OFDM, CP-OFDM and the measured signal. On the other hand, the measured signal has a higher FDR than CP-OFDM in the guard band above 50 MHz, because CP-OFDM with a rectangular pulse entails an intrinsically relatively high OOBE.

Figs. 20 and 21 are obtained by assuming a linearized power amplifier. However, the amplified signals can undergo in-band and out-of-band nonlinear distortion [37]–[39]. Due to this phenomenon, larger guard bands may be required to achieve the target FDR in Fig. 21 [20].

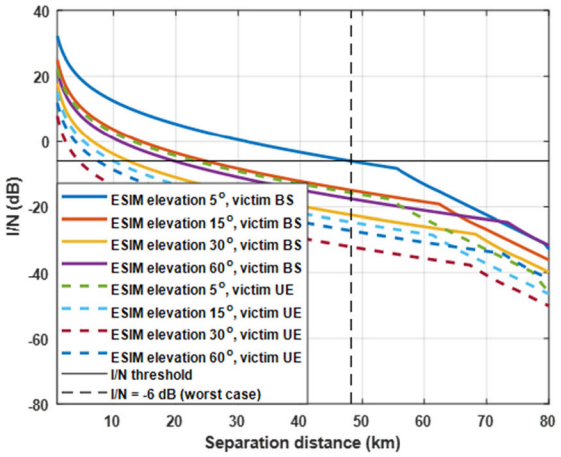

FIGURE 22. *I*/*N* of IMT-2020 with M-ESIM interference in zero guard band (MCL method).

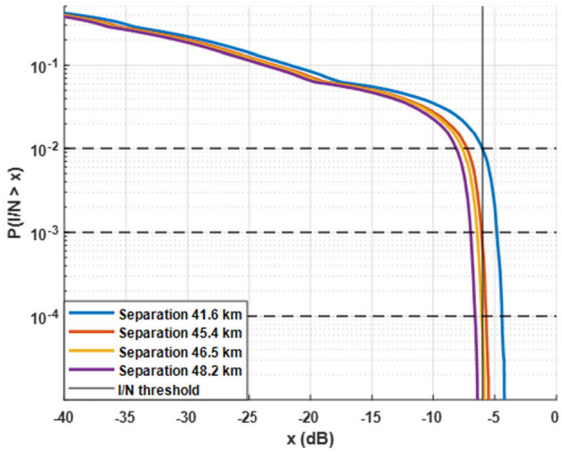

FIGURE 23. *I*/*N* CCDF of IMT-2020 BS with M-ESIM interference for various separation distances in zero guard band and the 5° ESIM elevation angle (MC method).

VI. SIMULATION PARAMETER AND RESULTS

Using the MCL method, the I/N of a single IMT-2020 BS and UE disrupted by an ESIM transmitter was first calculated, where the maximum antenna gain of the BS and UE are assumed considering harsh environments. The IMT-2020 network was then simulated with which the ESIM transmitter interferes, and analyzed the probability distribution of the I/N and throughput loss by using the MC method. Representative results are illustrated by Figs 22 to 34; all results are detailed in Tables 6 to 9. Tables 4 and 5 represent the simulation parameters of the ESIM and 5G systems.

A. M-ESIM INTERFERING WITH IMT-2020

Considering the MCL method, the separation distance is defined as the distance between the antenna of an IMT-2020 BS (or UE) and an M-ESIM, whereas it is defined as the distance from the border of an IMT-2020 network to an M-ESIM in the MC method.

TABLE 4. Parameters of IMT-2020.

Parameter	Value		Unit
	BS	UE	
Frequency	27.5		GHz
Bandwidth	200		MHz
Distribution density	30 BSs	100 UEs	/km^2
Antenna Height	6	1.5	m
Downtilt	10	0	Degree
Element gain	5		dBi
Antenna array	8 x 8	4 x 4	Row x Column
Ohmic loss	3		dB
Body loss	0	4	dB
Noise figure	10		dB
I/*N* threshold	-6	-6	dB

TABLE 5. Parameters of ESIM.

Parameter	Value	Unit
Frequency	27.5	GHz
Bandwidth	90	MHz
Antenna height	M-ESIM: 40 L-ESIM: 6 A-ESIM: Altitude	m
Elevation Angle	5, 15, 30, 60	Degree

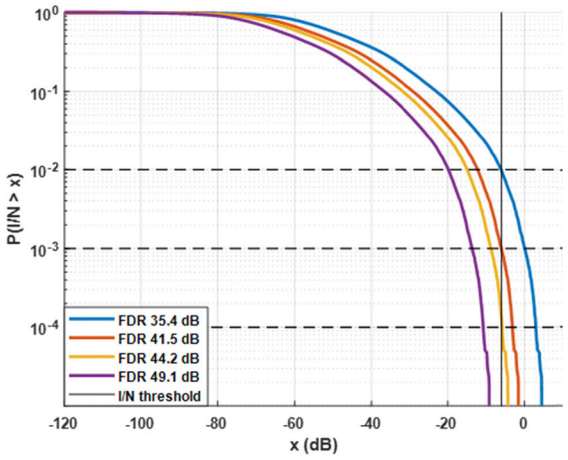

FIGURE 24. *I*/*N* CCDF of the IMT-2020 BS with M-ESIM interference for various FDRs in the separation distance of 1km and the 5° ESIM elevation angle (MC method).

1) INTERFERENCE TO NOISE RATIO

Fig. 22 presents the I/N value of the IMT-2020 BS and UE with which the M-ESIM interferes for various elevation angles of an M-ESIM antenna. The I/N values are calculated by the MCL method that adopts the measured waveform of a commercial ESIM device with a zero guard band. As indicated by the blue curve in Fig. 22, for *the worst case*, where the BS is a victim system and the ESIM antenna elevation angle is 5°, the minimum separation distance satisfying the

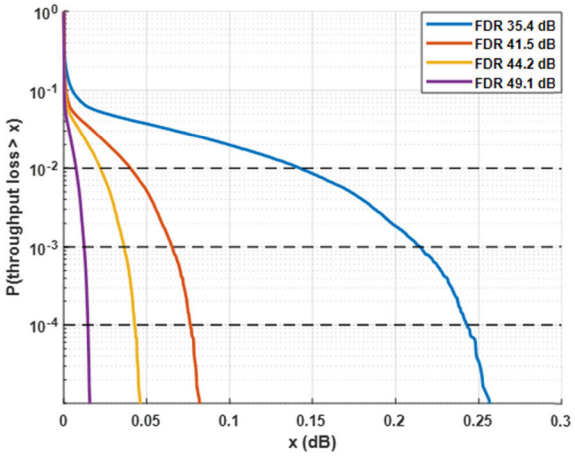

FIGURE 25. Throughput loss CCDF of the IMT-2020 BS with M-ESIM interference for various FDRs in the separation distance of 1km and the 5° ESIM elevation angle (MC method).

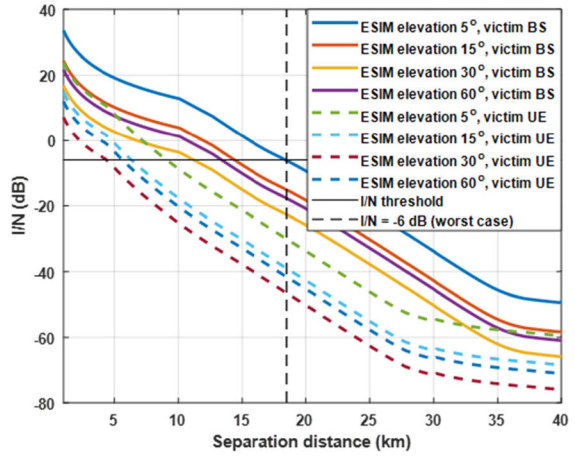

FIGURE 26. *I*/*N* of IMT-2020 with L-ESIM interference in zero guard band (MCL method).

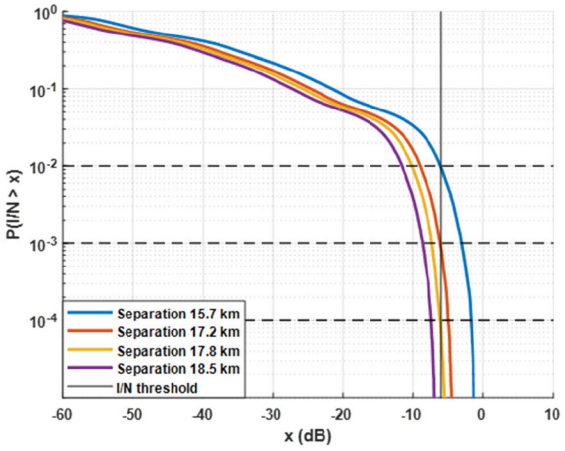

FIGURE 27. *I*/*N* CCDF of IMT-2020 BS with L-ESIM interference for various separation distances in zero guard band and the 5° ESIM elevation angle (MC method).

I/N threshold of -6 dB is 48.2 km. Overall, the interference power at the BS is higher than that at the UE for the same elevation angle, because the MCL method adopts

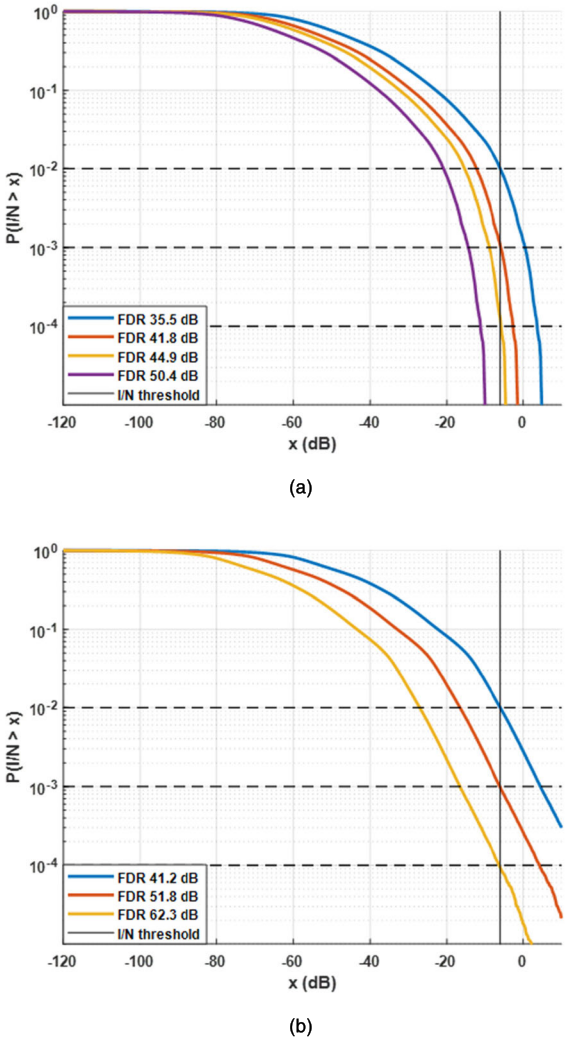

FIGURE 28. *I*/*N* CCDF of the IMT-2020 BS with L-ESIM interference for various FDRs and the 5° ESIM elevation angle (MC method): (a) outside IMT network, (b) inside IMT network.

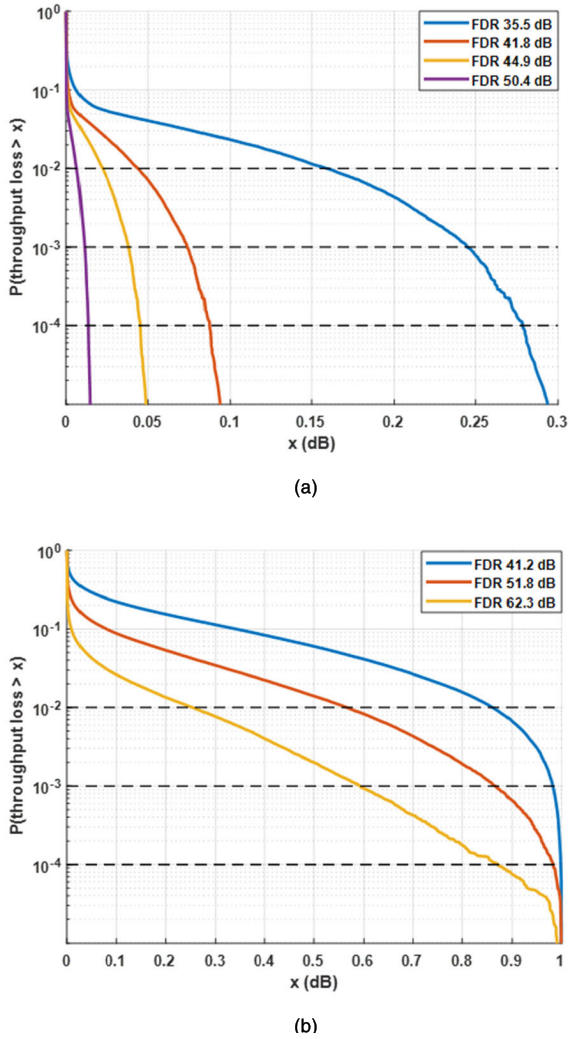

FIGURE 29. Throughput loss CCDF of the IMT-2020 BS with L-ESIM interference for various FDRs and the 5° ESIM elevation angle (MC method): (a) outside IMT network, (b) inside IMT network.

the maximum antenna gain of the BS and UE. In addition, the higher the ESIM elevation angle, the less interference. Meanwhile, the interference for the elevation angle of 30° is lower than for 60°, because the ESIM EIRP is saturated up to −10 dBW/40kHz above the off-axis angle of 48°, as shown in Fig. 13.

Table 6 presents more varied results of the MCL method: the minimum separation distance for the zero guard band, as well as the FDR and corresponding guard band required for the minimum separation distance of 1 km. For *the worst case* (i.e. the BS, 5° elevation angle), both, the CP-OFDM and windowed-OFDM required a minimum separation distance of approximately 24 km, meanwhile the measured signal required a significantly longer distance, 48.2 km. In addition, an FDR of 49.1 dB is required for the 1 km distance; a corresponding guard band of the measured signal, CP-OFDM, and windowed-OFDM was 57.2 MHz, 179.4 MHz, and 28.6 MHz, respectively. Here, the FDR of CP-OFDM was confirmed to be higher than that of the measured signal for a relatively small guard band; this was reversed for a large guard band as presented in Fig. 21.

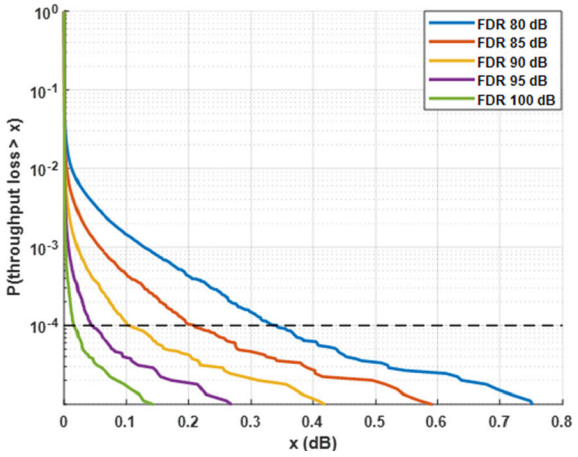

FIGURE 30. Throughput loss CCDF of the IMT-2020 BS with L-ESIM interference for relatively high FDRs and the 5° ESIM elevation angle (MC method): inside IMT network.

TABLE 6. MCL results of M-ESIM interfering with IMT-2020.

Elevation angle	Waveforms	Maritime ESIM					
		Victim system : BS			Victim system : UE		
		Minimum separation distance (km) for zero guard band	Required FDR for 1 km (dB)	Guard band (MHz)	Minimum separation distance (km) for zero guard band	Required FDR for 1 km (dB)	Guard band (MHz)
5°	Measured signal	48.2	49.1	57.2	23.2	39.5	47.4
	CP-OFDM	23.6		179.4	9.3		24.1
	Windowed OFDM	23.2		28.6	9.1		19
10°	Measured signal	35.2	45.0	53	15.4	35.4	43.3
	CP-OFDM	15.7		76	5.7		16.7
	Windowed OFDM	21.4		24.5	5.6		14.9
15°	Measured signal	24.8	40.8	48.6	9.9	31.1	38.9
	CP-OFDM	10.1		25.7	3.5		11.4
	Windowed OFDM	9.9		20.3	3.4		10.6
20°	Measured signal	18.9	37.7	45.6	7.1	28.1	35.5
	CP-OFDM	7.3		20.3	2.5		8.1
	Windowed OFDM	7.2		17.2	2.4		7.6
25°	Measured signal	15	35.3	43.2	5.5	25.7	32.6
	CP-OFDM	5.6		16.6	1.9		5.6
	Windowed OFDM	5.5		14.9	1.8		5.2
30°	Measured signal	12.4	33.4	41.2	4.4	23.7	29.9
	CP-OFDM	4.5		14.1	1.5		3.5
	Windowed OFDM	4.4		12.9	1.4		3.3
35°	Measured signal	10.5	31.7	39.6	3.7	22.1	27.3
	CP-OFDM	3.8		12.1	1.3		1.8
	Windowed OFDM	3.7		11.3	1.2		1.6
40°	Measured signal	9	30.3	38.1	3.1	20.6	24.9
	CP-OFDM	3.2		10.5	1.1		4
	Windowed OFDM	3.1		9.8	1.1		2
45°	Measured signal	7.9	29.0	36.7	2.7	19.4	22.5
	CP-OFDM	2.8		9.1	<1		0
	Windowed OFDM	2.7		8.6	<1		0
50°	Measured signal	19.8	38.5	46.3	7.6	28.8	36.4
	CP-OFDM	7.8		21.7	2.7		8.9
	Windowed OFDM	7.6		18	2.6		8.3
55°	Measured signal	19.8	38.5	46.3	7.6	28.8	36.4
	CP-OFDM	7.8		21.7	2.7		8.9
	Windowed OFDM	7.6		18	2.6		8.3
60°	Measured signal	19.8	38.5	46.3	7.6	28.8	36.4
	CP-OFDM	7.8		21.7	2.7		8.9
	Windowed OFDM	7.6		18	2.6		8.3

Figure 23 presents the complementary cumulative distribution function (CCDF) of I/N (or referred to as the exceeding probability) at the IMT-2020 BS obtained through the MC method for various separation distances and the 5° ESIM elevation angle. The probability of exceeding the I/N threshold of -6 dB, denoted by P($I/N > -6$dB), is 10^{-2} for the separation of 41.6 km less than the minimum separation distance of 48.2 km calculated by the MCL method. Furthermore, considering the separation of 48.2 km, P($I/N > -6$ dB) is less than 10^{-5}. Likewise, in Fig. 24, P($I/N > -6$ dB) with the 1 km separation is less than 10^{-5} for the FDR of 49.1 dB that is calculated by the MCL method. In summary, the MC method using stochastic interference analysis reduces the minimum separation distance and FDR with a proper exceeding probability, compared to the MCL method.

Table 7 presents the FDR obtained in the same way as in Fig. 24 for various ESIM elevation angles, and the corresponding guard band of the three waveforms. These values are useful for the IMT and ESIM system designer to select the exceeding probability and guard band for fulfilling adjacent channel compatibility.

2) THROUGHPUT LOSS

Fig. 25 presents the throughput loss CCDF of the IMT-2020 BS in the same conditions as in Fig. 24. For the FDR of 35.4 dB, the value x satisfying P(throughput loss $>$ x) $= 0.01$ is smaller than 0.15. In addition, P(throughput loss $>$ x) is less than 10^{-5} for all other FDRs. Namely, an increase in FDR can improve the quality of the interfering IMT-2020 service, but has the disadvantage of using a wider guard band or a filter with a sharp cut off. Although there is

TABLE 7. MC I/N results of IMT-2020 due to the interference of M-ESIM and L-ESIM.

Elevation angle	Waveforms	Victim system : BS											
		P(I/N>-6dB)=0.01				P(I/N>-6dB)=0.001				P(I/N>-6dB)=0.0001			
		M-ESIM		L-ESIM		M-ESIM		L-ESIM		M-ESIM		L-ESIM	
		FDR (dB)	Guard Band (MHz)	FDR (dB)	Guard Band (MHz)	FDR (dB)	Guard Band (MHz)	FDR (dB)	Guard Band (MHz)	FDR (dB)	Guard Band (MHz)	FDR (dB)	Guard Band (MHz)
5°	Measured signal	35.4	43.3	35.5	43.4	41.5	49.4	41.8	49.8	44.2	52.2	44.9	74.6
	CP-OFDM		16.8		16.9		31.6		33.5		62.5		52.9
	Windowed OFDM		15		15.1		21.1		21.4		23.8		24.5
10°	Measured signal	32.3	40.2	32.6	40.5	38.3	46.2	38.6	46.5	41.2	49.1	41.4	49.3
	CP-OFDM		12.9		13.2		21.5		22.1		30		31.1
	Windowed OFDM		11.9		12.2		17.9		18.2		20.8		21
15°	Measured signal	29.1	36.8	29.2	36.9	34.8	42.7	34.9	42.8	37.5	45.4	37.4	45.3
	CP-OFDM		9.2		9.3		16		16.1		20		19.9
	Windowed OFDM		8.7		8.8		14.4		14.5		17.1		17
20°	Measured signal	26.6	33.8	26.8	34.1	31.9	39.8	32.2	40.1	34.9	42.8	34.6	42.5
	CP-OFDM		6.6		6.8		12.4		12.7		16.1		15.7
	Windowed OFDM		6.2		6.4		11.5		11.8		14.5		14.2
25°	Measured signal	24.7	31.3	24.9	31.6	30	37.8	30.1	37.9	32.5	40.4	32.3	40.2
	CP-OFDM		4.6		4.8		10.2		10.3		13.1		12.9
	Windowed OFDM		4.3		4.5		9.6		9.7		12.1		11.9
30°	Measured signal	23.1	29	23.2	29.1	28.1	35.7	28.2	35.8	30.9	38.8	30.7	38.5
	CP-OFDM		2.9		3		8.2		8.3		11.2		11
	Windowed OFDM		2.7		2.8		7.7		7.8		10.5		10.3
35°	Measured signal	21.9	27.1	21.9	27.1	27.1	34.4	26.9	34.2	30.1	37.9	29.6	37.3
	CP-OFDM		1.7		1.7		7.1		6.9		10.3		9.8
	Windowed OFDM		1.5		1.5		6.7		6.5		9.7		9.2
40°	Measured signal	21.1	25.7	21.2	25.9	27.9	35.4	27.7	35.2	30.9	38.8	30.8	38.6
	CP-OFDM		0.9		1		7.9		7.7		11.2		11.1
	Windowed OFDM		0.6		0.8		7.5		7.3		10.5		10.4
45°	Measured signal	25.8	32.8	25.3	32.1	31.1	39	31.2	39.1	33	40.9	33.3	41.2
	CP-OFDM		5.7		5.2		11.5		11.6		13.7		14.1
	Windowed OFDM		5.4		4.9		10.7		10.8		12.6		12.9
50°	Measured signal	29.4	37.1	29.3	37	33.7	41.6	33.6	41.5	36.4	44.3	35.7	43.6
	CP-OFDM		9.6		9.5		14.6		14.4		18.3		17.2
	Windowed OFDM		9		8.9		13.3		13.2		16		15.3
55°	Measured signal	29.4	37.1	29.4	37.1	33.7	41.6	33.6	41.5	36.4	44.3	35.7	43.6
	CP-OFDM		9.6		9.6		14.6		14.4		18.3		17.2
	Windowed OFDM		9		9		13.3		13.2		16		15.3
60°	Measured signal	29.4	37.1	29.4	37.1	33.7	41.6	33.6	41.5	36.4	44.3	35.7	43.6
	CP-OFDM		9.6		9.6		14.6		14.4		18.3		17.2
	Windowed OFDM		9		9		13.3		13.2		16		15.3

not an authorized criterion of the throughput loss for ensuring the compatibility of the two systems, the guard band could be set by determining the throughput loss acceptable to the IMT service.

Table 8 presents the throughput loss of the BS for various elevation angles including the results above. In Table 7, for the ESIM elevation angle of 10°, the FDR satisfying P(X $>$ −6dB) $= 10^{-2}$, 10^{-3}, and 10^{-4} is 32.3 dB, 38.3 dB, and 41.2 dB, respectively. When the FDR of 32.3 dB is applied to Table 8, the value of x satisfying P(throughput loss $>$ x) $= 10^{-2}$, 10^{-3}, and 10^{-4} is 0.14, 0.2, and 0.22, respectively. The data presented in Table 8 can be used as useful information for setting the FDR and the guard band to satisfy the target loss value for various ESIM operating environments and antenna elevation angles.

B. L-ESIM INTERFERING WITH IMT-2020

The L-ESIM results were also structured identically to the previous chapter for M-ESIM. One difference was that the MC analysis for the IMT network was conducted, given the two positions of L-ESIM: outside and inside IMT network. For an L-ESIM outside the IMT network, the separation distance is measured from the border of the IMT network, whereas for an L-ESIM inside the IMT network, the IMT-2020 BS and UE are placed around the L-ESIM at least 10 m apart.

1) INTERFERENCE TO NOISE RATIO

The simulation results for the L-ESIM outside of the IMT network are presented in Figs. 26, 27, 28(a), and Tables 7, 8, and 9. Figure 26 presents the I/N of IMT-2020 BS and UE using the MCL method based on the

TABLE 8. MC throughput loss of IMT-2020 due to the interference of M-ESIM and L-ESIM.

Elevation angle	P(throughput loss>x)	Victim system : BS											
		P(I/N>-6dB)=0.01				P(I/N>-6dB)=0.001				P(I/N>-6dB)=0.0001			
		M-ESIM		L-ESIM		M-ESIM		L-ESIM		M-ESIM		L-ESIM	
		FDR (dB)	Throughput loss x	FDR (dB)	Throughput loss x	FDR (dB)	Throughput loss x	FDR (dB)	Throughput loss x	FDR (dB)	Throughput loss x	FDR (dB)	Throughput loss x
5°	0.01	35.4	0.14	35.5	0.16	41.5	0.04	41.8	0.04	44.2	0.02	44.9	0.02
	0.001		0.21		0.25		0.07		0.07		0.04		0.04
	0.0001		0.24		0.28		0.08		0.09		0.04		0.05
10°	0.01	32.3	0.14	32.6	0.14	38.3	0.04	38.6	0.04	41.2	0.02	41.4	0.02
	0.001		0.2		0.21		0.06		0.07		0.03		0.04
	0.0001		0.22		0.23		0.07		0.07		0.04		0.04
15°	0.01	29.1	0.12	29.2	0.13	34.8	0.04	34.9	0.04	37.5	0.02	37.4	0.02
	0.001		0.17		0.19		0.05		0.06		0.03		0.04
	0.0001		0.19		0.2		0.06		0.07		0.03		0.04
20°	0.01	26.6	0.1	26.8	0.11	31.9	0.03	32.2	0.04	34.9	0.02	34.6	0.02
	0.001		0.16		0.17		0.05		0.06		0.03		0.03
	0.0001		0.18		0.19		0.06		0.06		0.03		0.04
25°	0.01	24.7	0.1	24.9	0.1	30	0.03	30.1	0.03	32.5	0.02	32.3	0.02
	0.001		0.15		0.15		0.05		0.05		0.03		0.03
	0.0001		0.16		0.17		0.06		0.06		0.03		0.04
30°	0.01	23.1	0.09	23.2	0.17	28.1	0.03	28.2	0.03	30.9	0.02	30.7	0.02
	0.001		0.14		0.15		0.05		0.05		0.03		0.03
	0.0001		0.16		0.1		0.06		0.06		0.03		0.04
35°	0.01	21.9	0.08	21.9	0.1	27.1	0.03	26.9	0.03	30.1	0.01	29.6	0.02
	0.001		0.12		0.14		0.04		0.05		0.02		0.03
	0.0001		0.14		0.16		0.05		0.06		0.03		0.03
40°	0.01	21.1	0.07	21.2	0.08	27.9	0.02	27.7	0.02	30.9	0.01	30.8	0.01
	0.001		0.11		0.12		0.03		0.03		0.01		0.02
	0.0001		0.13		0.14		0.03		0.04		0.02		0.02
45°	0.01	25.8	0.02	25.3	0.02	31.1	0.01	31.2	0.01	33	0	33.3	0
	0.001		0.03		0.04		0.01		0.01		0.01		0.01
	0.0001		0.04		0.04		0.01		0.01		0.01		0.01
50°	0.01	29.4	0.07	29.3	0.08	33.7	0.03	33.6	0.03	36.4	0.02	35.7	0.02
	0.001		0.1		0.12		0.04		0.05		0.02		0.03
	0.0001		0.12		0.14		0.05		0.06		0.03		0.04
55°	0.01	29.4	0.07	29.4	0.08	33.7	0.03	33.6	0.03	36.4	0.02	35.7	0.02
	0.001		0.1		0.12		0.04		0.05		0.02		0.03
	0.0001		0.12		0.13		0.05		0.06		0.03		0.04
60°	0.01	29.4	0.07	29.4	0.08	33.7	0.03	33.6	0.03	36.4	0.02	35.7	0.02
	0.001		0.1		0.12		0.04		0.05		0.02		0.03
	0.0001		0.12		0.13		0.05		0.06		0.03		0.04

measured waveform of a commercial ESIM device with a zero guard band. Here, *the worst case* is indicated by the blue curve where the ESIM antenna elevation angle is 5° and the victim system is BS, such as the M-ESIM. The minimum separation distance satisfying the I/N threshold is approximately 18.5 km. Table 9 presents more various results of the MCL method including the results in Fig. 26. Compared to the M-ESIM, the separation distance is short due to a large propagation loss in a land area, as shown in Fig. 16.

Figure 27 presents the I/N CCDF obtained by the MC method in *the worst case*, where P($I/N > -6$dB) is less than 10^{-5} at the separation distance of 18.5 km which is obtained in Fig. 26 by the MCL method. In addition, P($I/N > -6$dB) $= 10^{-2}$, 10^{-3}, and 10^{-4} at the separation distance of 15.7 km, 17.2 km, and 17.8 km, respectively. Figures 28 (a) and (b) present the I/N CCDF for the FDRs satisfying P($I/N > -6$dB) $= 10^{-2}$, 10^{-3}, and 10^{-4} in the case of L-ESIM outside and inside the IMT network, respectively. In Fig. 28(a), given the separation distance of 1 km, P($I/N > -6$dB) is less than 10^{-5} for the FDR of 50.4 dB. Here, the 50.4 is a value calculated by the MCL method to satisfy the I/N threshold at the 1 km separation. As with the results of M-ESIM, the results in Figs. 26, 27, and 28(a) indicate that the separation distances less than the values obtained by the MCL method would be acceptable with a proper exceeding probability.

As shown in Fig. 28(b), higher FDRs are required for P(X > -6dB) $= 10^{-2}$, 10^{-3}, and 10^{-4} compared to those in Fig. 28(a). This is due to the minimum separation distance between the L-ESIM and IMT-2020 BS set to 10 m; therefore, the propagation loss is very low.

TABLE 9. MCL results of L-ESIM interfering with IMT-2020.

Elevation angle	Waveforms	Land ESIM					
		Victim system: BS			Victim system: UE		
		Minimum separation distance (km) for zero guard band	Required FDR for 1 km (dB)	Guard band (MHz)	Minimum separation distance (km) for zero guard band	Required FDR for 1 km (dB)	Guard band (MHz)
5°	Measured signal	18.5	50.4	58.5	9.2	40.7	48.6
	CP-OFDM	14.3		226.4	6.3		27.9
	Windowed OFDM	14.2		30	6.2		20.3
10°	Measured signal	16.3	45.7	53.7	7.7	36.0	43.9
	CP-OFDM	12.5		89.6	5.1		17.6
	Windowed OFDM	12.4		25.2	5		15.6
15°	Measured signal	14.5	41.2	49.1	6.4	32.5	40.4
	CP-OFDM	10.3		30	3.6		13.1
	Windowed OFDM	10.2		20.8	3.5		12.1
20°	Measured signal	13.3	38.0	46	5.6	28.4	35.9
	CP-OFDM	7.5		21	2.6		8.4
	Windowed OFDM	7.4		17.6	2.5		7.9
25°	Measured signal	12.2	35.6	43.5	5	25.9	33
	CP-OFDM	5.8		17.1	2		5.8
	Windowed OFDM	5.7		15.2	1.9		5.5
30°	Measured signal	11.3	33.6	41.5	4.4	22.9	28.7
	CP-OFDM	4.6		14.4	1.6		2.8
	Windowed OFDM	4.5		13.2	1.5		2.5
35°	Measured signal	10.5	31.9	39.8	3.8	22.2	27.6
	CP-OFDM	3.8		12.4	1.3		2
	Windowed OFDM	3.7		11.5	1.3		1.8
40°	Measured signal	9.3	30.5	38.3	3.2	20.8	25.2
	CP-OFDM	3.3		10.8	1.1		0.4
	Windowed OFDM	3.2		10	1.1		0.6
45°	Measured signal	8.1	29.2	36.9	2.8	19.5	22.8
	CP-OFDM	2.8		9.3	0		0
	Windowed OFDM	2.8		8.8	0		0
50°	Measured signal	13.4	38.5	46.4	5.7	28.8	36.4
	CP-OFDM	8		21.9	2.7		8.9
	Windowed OFDM	7.8		18.1	2.6		8.4
55°	Measured signal	13.4	38.5	46.4	5.7	28.8	36.4
	CP-OFDM	8		21.9	2.7		8.9
	Windowed OFDM	7.8		18.1	2.6		8.4
60°	Measured signal	13.4	38.5	46.4	5.7	28.8	36.4
	CP-OFDM	8		21.9	2.7		8.9
	Windowed OFDM	7.8		18.1	2.6		8.4

2) THROUGHPUT LOSS

Given the separation distance of 1 km, Fig. 29(a) presents the throughput loss CCDF for the FDRs similar to Fig 28(a). When an FDR of 41.8 dB is applied, the P(throughput loss $>$ 0.05) is less than 10^{-2}. Table 8 presents the throughput loss of the BS for various elevation angles including the results above.

Figure 29(b) presents the throughput loss CCDF for the FDRs similar to Fig 28(b), i.e. the case of L-ESIM inside the IMT network. Note, the throughput loss is significant (i.e. P(throughput loss $>$ 0.25) $= 10^{-2}$) despite a relatively high FDR of 62.3 dB, compared to the CCDF in Fig. 28(a). This occurs because some victim BSs exceeding the I/N threshold could receive a significantly high interference from the L-ESIM. Therefore, not only the I/N, a typical metric, but also the throughput loss could be examined in a compatibility study. As shown in Fig. 30, a significantly higher FDR is required to ensure an acceptable throughput loss, e.g. P(throughput loss $>$ 0.3) $= 10^{-4}$ for the FDR of 80 dB. However, an FDR of 80 dB cannot be reached by frequency separation, given the OOBE of the measured signal and CP-OFDM. Practically, this FDR can be achieved by the windowed-OFDM waveform of the ESIM with a guard band above 59.6 MHz.

C. A-ESIM INTERFERING WITH IMT-2020

Fig. 31 presents the I/N calculated by the MCL method along the visible path of the A-ESIM with an altitude of 6.4 km, where there is a zero fuselage loss and the measured waveform of ESIM with a zero guard band is applied. The I/N value satisfies the I/N requirement for all points on the visible path. In addition, the I/N curves of adding fuselage

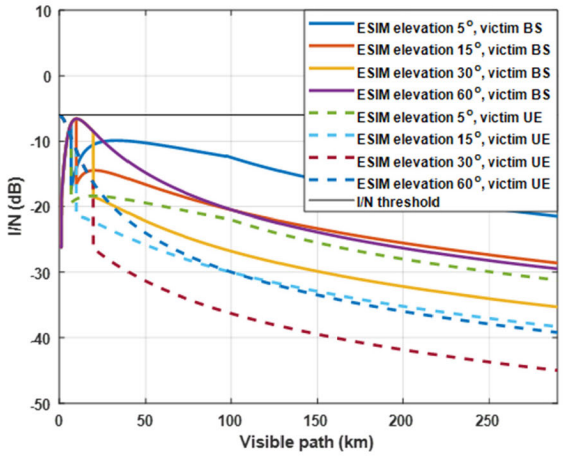

FIGURE 31. *I*/*N* of IMT-2020 with A-ESIM interference in zero guard band and the altitude of 6.4 km.

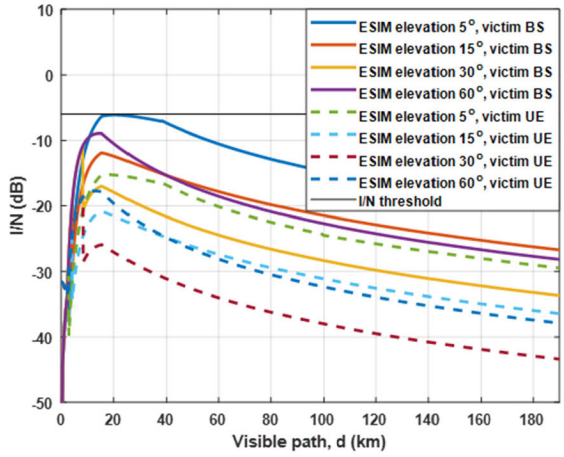

FIGURE 32. *I*/*N* of IMT-2020 with A-ESIM interference reduced by fuselage loss in zero guard band and the altitude of 2.7 km.

loss for the same environment is given in Fig. 32, where an altitude of 2.7 km is sufficient to fulfill the I/N requirement. Although not shown in the figures, the minimum altitude is 2.1 km for both the CP-OFDM and windowed-OFDM without fuselage loss, and it is 930 m for both with fuselage loss.

The A-ESIM is a system for providing wireless services to passengers in an aircraft. Considering that the altitude of the domestic and international flights is at least 6.7 km or more, it is expected to be compatible with the IMT-2020 regardless of the fuselage loss, excluding takeoff and landing.

VII. CONCLUSION

A general model of a multi-tier IMT-2020 cellular network in a coexistence study with other systems is presented, and the model is applied for assessing the effect of adjacent channel interference from three types of ESIM within the 27.5–29.5 GHz band. For quantifying the interference reduction produced by the IMT-2020 receiver selectivity and ESIM transmitter OOB, a mathematical expression of the FDR for varying the guard band was derived, using the measured transmission spectrum of the actual ESIM and the practical receiver filter of the IMT-2020. In addition, the CP-OFDM and windowed-OFDM waveforms are proposed to efficiently use frequency resources. The windowed-OFDM has a higher FDR than the measured signal for all guard bands, however, the CP-OFDM has a higher performance in the guard band below 50 MHz.

Considering the M-ESIM interfering with a BS, the required guard band (calculated by MCL method) of a measured signal, CP-OFDM, and windowed-OFDM is 36.7–57.2 MHz, 9.1–179.4 MHz, and 8.6–28.6 MHz, respectively, at a 1 km separation. In addition, the values are 36.9–58.5 MHz, 9.3–226.4 MHz, and 8.8–30 MHz for L-ESIM. For both, M-ESIM and L-ESIM, when using the MC method, the I/N criterion could be satisfied with an FDR that is approximately 15 dB smaller than the FDR calculated by the MCL method for an I/N excess probability of 1%. Considering the A-ESIM, a spectral coexistence is sufficiently possible, except for the takeoff and landing of an aircraft.

The significant amount of results presented in this study will be able to be used as technical data for the compatibility evaluation of IMT-2020 and ESIM with different elevation angles globally. WRC-19 adopted the WRC-23 agenda item 1.16 to protect services in the 27.5–29.1 GHz band from non-GSO ESIM. It is expected that this study can be applied to the interference scenario of the corresponding agenda. In the future, we will conduct a study to mathematically derive PSD and FDR of the OFDM waveforms applying the effect of the nonlinear distortion the power amplifier.

REFERENCES

[1] ECC. *ECC Newsletter*. Accessed: Jun. 1, 2019. [Online]. Available: http://apps.cept.org/eccnews/oct-2016

[2] Inmarsat. *Earth Station in Motion Ka-Band*. Accessed: Jun. 1, 2019. [Online]. Available: https://www.inmarsat.com/blog/earth-stations-in-motion-in-fss-kaband

[3] *Use of the Frequency Bands 19.7-20.2 GHz and 29.5-30 GHz by Earth Stations in Motion Communicating With Geostationary Space Stations in the Fixed-Satellite Service, World Radiocommunication Conference, ITU*, document Resolution 156, 2015.

[4] *Use of the Frequency Bands 17.7-19.7 GHz (Space-to-Earth) and 27.5-29.5 GHz (Earth-to-Space) by Earth Stations in Motion Communicating With Geostationary Space Stations in the Fixed-Satellite Service, World Radiocommunication Conference, ITU*, document Resolution 158, 2015.

[5] *Operation of Earth Stations in Motion Communicating With Geostationary Space Stations in the Fixed-Satellite Service Allocations at 17.7-19.7 GHz and 27.5-29.5 GHz*, document Rep ITU-R S.2464, Jul. 2019.

[6] *Use of the Frequency Bands 17.7-19.7 GHz and 27.5-29.5 GHz by Earth Stations in Motion Communicating With Geostationary Space Stations in the Fixed-Satellite Service, World Radiocommunication Conference, ITU*, document Resolution 169, 2019.

[7] *IMT Vision-Framework and Overall Objectives of the Future Development of IMT for 2020 and Beyond*, document Rec. ITU-R M.2083, Sep. 2015.

[8] *Studies on Frequency-Related Matters for International Mobile Telecommunications Identification Including Possible Additional Allocations to the Mobile Services on a Primary Basis in Portion(s) of the Frequency Range Between 24.25 and 86 GHz for the Future Development of International Mobile Telecommunications for 2020 and Beyond, World Radiocommunication Conference, ITU*, document Resolution 238, 2015.

[9] *Sharing and Compatibility of the FSS and IMT Operating in the 24.25-27.5 GHz Frequency range*, ITU-R Attachment 3 to Annex 3 to document 5-1/478-E, Sep. 2018.

[10] ECC, "A comparison of the minimum coupling loss method, enhanced minimum coupling loss method and the Monte-Carlo simulation," CEPT, Menton, France, ERC Rep. 101, 1999.

[11] W.-G. Chung, H.-S. Jo, H.-G. Yoon, J.-W. Lim, J.-G. Yook, and H.-K. Park, "Advanced MCL method for sharing analysis of IMT-advanced systems," *Electron. Lett.*, vol. 42, no. 21, pp. 1234–1235, Oct. 2006.

[12] H.-S. Jo, H.-G. Yoon, J. Lim, and J.-G. Yook, "An advanced MCL method for assessing interference potential of OFDM-based systems beyond 3G with dynamic power allocation," in *Proc. Eur. Conf. Wireless Technol.*, Manchester, U.K., Sep. 2006, pp. 39–42.

[13] W. A. Hassan, H.-S. Jo, S. Ikki, and M. Nekovee, "Spectrum-sharing method for co-existence between 5G OFDM-based system and fixed service," *IEEE Access*, vol. 7, pp. 77460–77475, 2019.

[14] Y. S. Cho, J. Kim, W. Y. Yang, and C.-G Kang, *MIMO-OFDM Wireless Communications With MATLAB*. Singapore: Wiley (Asia) Pte. Ltd., 2010.

[15] Y. Cho, H. Kim, E. E. Ahiagbe, and H.-S. Jo, "Spectral coexistence of IMT-2020 with fixed-satellite service in the 27-27.5 GHz band," in *Proc. Int. Conf. Inf. Commun. Technol. Converg. (ICTC)*, Oct. 2018, pp. 1–6.

[16] Y. Cho, H.-K. Kim, M. Nekovee, and H.-S. Jo, "Coexistence of 5G with satellite services in the millimeter-wave band," *IEEE Access*, vol. 8, pp. 163618–163636, 2020.

[17] H.-K. Son and Y.-J. Chong, "Analysis of the interference effects from maritime Earth station in motion to 5G mobile service," in *Proc. Int. Conf. Inf. Commun. Technol. Converg. (ICTC)*, Oct. 2017, pp. 1225–1228.

[18] H.-K. Kim, Y. Cho, E. E. Ahiagbe, and H.-S. Jo, "Adjacent channel interference from maritime Earth station in motion to 5G mobile service," in *Proc. Int. Conf. Inf. Commun. Technol. Converg. (ICTC)*, Oct. 2018, pp. 1164–1169.

[19] H.-K. Kim, Y. Cho, D. K. Tettey, and H.-S. Jo, "Adjacent channel compatibility between OFDM-based Earth station in motion and 5G," in *Proc. IEEE Globecom Workshops (GC Wkshps)*, Dec. 2019, pp. 1–6.

[20] J. Park, E. Lee, S.-H. Park, S.-S. Raymond, S. Pyo, and H.-S. Jo, "Modeling and analysis on radio interference of OFDM waveforms for coexistence study," *IEEE Access*, vol. 7, pp. 35132–35147, 2019.

[21] *Study on New Radio Access Technology: Radio Frequency (RF) and Co-Existence Aspects*, document TR 38.803, 3GPP, Sep. 2017.

[22] *Modelling and Simulation of IMT Networks and Systems for use in Sharing and Compatibility Studies*, document Rec. ITU-R M.2101, Feb. 2017.

[23] *Radio Frequency (RF) System Scenarios*, document TR 25.942, 3GPP, Jan. 2016.

[24] *The Harmonized Use, Free Circulation and Exemption From Individual Licensing of Earth Stations on Mobile Platforms (ESOMPs) Within the Frequency Bands 17.3–20.2 GHz and 27.5–30.0 GHz*, ECC Decision, Mar. 2013, vol. 13, no. 1.

[25] H. K. Kim, Y. Cho, and H. S. Jo, "Interference analysis for compatibility evaluation between aeronautical Earth station in motion and 5G mobile communications," *JKIEES*, vol. 30, no. 9, pp. 733–741, Sep. 2019.

[26] *Maximum Permissible Levels of Off-Axis e.i.r.p Density From Earth Stations in Geostationary-Satellite Orbit Metworks Operating in the Fixed-Satellite Service Transmitting in the 6 GHz, 13 GHz, 14 GHz and 30 GHz frequency bands*, document Rec. ITU-R S.524-9, 2006.

[27] *Frequency and Distance Separations*, document Rec. ITU-R SM.337-6, 2008.

[28] *Prediction Procedure for the Evaluation of Interference Between Stations on the Surface of the Earth at Frequencies Above About 0.1 GHz*, document Rec. ITU-R P.452-16, 2016.

[29] *Determination of the Interference Potential Between Earth Stations of the Fixed-Satellite Service and Stations in the Fixed Service*, document Rec. ITU-R SF.1006, Apr. 1993.

[30] *Considerations in the Development of Criteria for Sharing Between the Terrestrial Fixed Service and Other Services*, document Rec. ITU-R F.758-4, Jan. 2005.

[31] *Calculation of Free-Space Attenuation*, document Rec. ITU-R P.525-4, Aug. 2019.

[32] RF Tools. *LC Filters Design Tool*. Accessed: Jun. 15, 2019. [Online]. Available: https://rf-tools.com/lc-filter

[33] M. Batariere, K. Baum, and T. P. Krauss, "Cyclic prefix length analysis for 4G OFDM systems," in *Proc. IEEE 60th Veh. Technol. Conf. (VTC-Fall)*, Sep. 2004, pp. 543–547.

[34] A. D. S. Jayalath and C. Tellambura, "Reducing the out-of-band radiation of OFDM using an extended guard interval," in *Proc. IEEE 54th Veh. Technol. Conf. (VTC Fall)*, Oct. 2001, pp. 829–833.

[35] C. Liu and F. Li, "Spectrum modelling of OFDM signals for WLAN," *Electron. Lett.*, vol. 40, no. 22, pp. 1431–1432, Oct. 2004.

[36] ShareTechnote. *5G/NR-Frame Structure*. Accessed: Jun. 15, 2019. [Online]. Available: https://www.sharetechnote.com/html/5G/5G_FrameStructure.html

[37] T. Lee and H. Ochiai, "A simple characterization of power spectral density for nonlinearly amplified OFDM signals," in *Proc. IEEE Topical Conf. Power Modeling Wireless Radio Appl. (PAWR)*, Jan. 2014, pp. 88–90.

[38] J. Yli-Kaakinen, T. Levanen, S. Valkonen, K. Pajukoski, J. Pirskanen, M. Renfors, and M. Valkama, "Efficient fast-convolution-based waveform processing for 5G physical layer," *IEEE J. Sel. Areas Commun.*, vol. 35, no. 6, pp. 1309–1326, Jun. 2017.

[39] Y. Huang and B. Su, "Circularly pulse-shaped precoding for OFDM: A new waveform and its optimization design for 5G new radio," *IEEE Access*, vol. 6, pp. 44129–44146, Aug. 2018.

HYUN-KI KIM (Student Member, IEEE) received the B.S. and M.S. degrees in electronics and control engineering from Hanbat National University, Daejeon, South Korea, in 2018 and 2020, respectively. His current research interests are spectral compatibility/coexistence and interference mitigateon technique.

YEONGI CHO (Student Member, IEEE) received the B.S. and M.S. degrees in electronics and control engineering from Hanbat National University, Daejeon, South Korea, in 2018 and 2020, respectively, where he is currently pursuing the Ph.D. degree with the Department of Electronics and Control Engineering. His current research interests are interference analysis between wireless cellular and satellite service and wireless communication system structure, such as physical layer and channel modeling.

HAN-SHIN JO (Member, IEEE) received the B.S., M.S., and Ph.D. degrees in electrical and electronics engineering from Yonsei University, Seoul, South Korea, in 2001, 2004, and 2009, respectively. He was a Postdoctoral Research Fellow with the Wireless Networking and Communications Group, Department of Electrical and Computer Engineering, The University of Texas at Austin, from 2009 to 2011. He developed a long-term evolution base station in Samsung Electronics from 2011 to 2012. He has been a member of the Korea ITU-R Working Party 5-D Committee since 2016. He is currently an Associate Professor with the Department of Electronics and Control Engineering, Hanbat National University, Daejeon, South Korea. His current research interests are in coexistence study and spectrum sharing, and applications of stochastic geometry, optimization theory, and machine/reinforcement learning to wireless communications and networking.